POLITECNICO DI TORINO

Master of Science in

Energy and Nuclear Engineering

Master thesis

STUDY OF THE TECHNICAL FEASIBILITY OF A "LOHC HYDROGEN STORAGE AND SOFC SYSTEM" FOR AIRCRAFT APPLICATION

Advisor
Prof. Massimo Santarelli

Co-Advisor
Dott. Paolo Marocco
Dott.ssa Roberta Biga

Candidate
Davide Marcacini

Anno Accademico 2021/2022

TABLE OF CONTENTS

TABLE OF CONTENTS....2
ABSTRACT....6
LIST OF FIGURES....8
LIST OF TABLES....11
ACRONYMS....14
1. INTRODUCTION....16
2. H_2 STORAGE TECHNOLOGIES....17
2.1. COMPRESSED HYDROGEN....17
2.1.1. ADVANTAGES AND DISADVANTAGES OF CH_2....19
2.2. LIQUIFIED HYDROGEN....19
2.2.1. ADVANTAGES AND DISADVANTAGES OF LH2....20
2.3. LIQUID ORGANIC HYDROGEN CARRIER....21
2.3.1. ADVANTAGES AND DISADVANTAGES OF LOHCs....22
2.4. METAL HYDRIDES....23
2.4.1. ADVANTAGES AND DISADVANTAGES OF METAL HYDRIDES....24
3. STORAGE TECHNOLOGIES CONSIDERED....25
3.1. LOHC MATERIALS CONSIDERED....25
3.1.1. DEHYDROGENATION CONDITIONS OF LOHCs....26
3.1.2. DYNAMIC BEHAVIOR OF LOHCs DEHYDROGENATION....29
3.2. METAL HYDRIDE MATERIALS CONSIDERED....33
3.2.1. MH DEHYDROGENATION CONDITIONS....34

3.2.2. DYNAMIC BEHAVIOR OF MHs DEHYDROGENATION 40
3.3. CHOICE OF THE BEST TECHNOLOGY TO BE COUPLED WITH A FUEL CELL SYSTEM.....41
3.3.1. CHOICE OF THE BEST LOHC TECHNOLOGY.....41
3.3.1.1. DIBENZYLTOLUENE/PERHYDRO-DIBENZYLTOLUENE 43
4. FUEL CELL SYSTEM.....45
4.1. PROTON EXCHANGE MEMBRANE FUEL CELL (PEMFC).....45
4.1.1. PEMFC DYNAMIC BEHAVIOR.....47
4.2. SOLID OXIDE FUEL CELL (SOFC).....49
4.2.1. SOFC DYNAMIC BEHAVIOR.....51
4.3. CHOICE OF THE FUEL CELL TO BE COUPLED WITH THE H18-DBT/H0-DBT SYSTEM 52
5. ASPEN MODELING 54
5.1. H_2 RELEASE SYSTEM CONFIGURATION 54
5.2. SOLID OXIDE FUEL CELL SYSTEM CONFIGURATION.....56
5.2.1. SOFC SYSTEM.....56
5.2.2. SOFC THERMAL BALANCE 57
5.2.3. CALCULATOR BLOCKS.....59
5.2.3.1. C-INPUT 60
5.2.3.2. C-OXY 61
5.2.3.3. C-AIR 62
5.2.4. DESIGN SPECIFICATION 62
5.2.4.1. DS-AIR.....63
6. ALL-ELECTRIC CASE STUDY.....64
6.1. SCENARIO AND WORKING CONDITIONS 64
6.2. WEIGHT EVALUATION.....66

6.2.1. H18-DBT AND H0-DBT TANK 66
6.2.2. HORIZONTAL TUBE REACTOR 72
6.2.3. FLASH SEPARATOR 75
6.2.4. LOHC PUMP 77
6.2.5. SOFC STACK 77
6.2.6. COMPRESSOR AND HEAT EXCHANGERS 78
6.3. TOTAL WEIGHT AND GRAVIMETRIC INDEX OF H_2 STORAGE 79
6.4. CONSIDERATIONS 80
7. SENSITIVITY ANALYSIS 84
7.1. FUEL UTILIZATION 84
7.2. FLUID PRESSURE ENTERING THE SOFC STACK 90
7.3. PRESSURE DROP INSIDE THE HEAT EXCHANGERS 94
7.4. CONSIDERATIONS ON THE FINAL CONFIGURATION OF THE ALL-ELECTRIC CASE 96
8. HYBRIDIZATION OF THE ATR-72 600 99
8.1. 80% OF HYBRIDIZATION 99
8.1.1. FEASIBILITY EVALUATION OF THE 80% HYBRIDIZATION CASE 102
8.2. 60% OF HYBRIDIZATION 103
8.2.1. FEASIBILITY EVALUATION OF THE 60% HYBRIDIZATION CASE 105
8.3. 40% IBRIDIZATION 106
8.3.1. FEASIBILITY EVALUATION OF THE 40% HYBRIDIZATION CASE 108
8.4. 20% IBRIDIZATION 109
8.4.1. FEASIBILITY EVAULATION OF THE 20% HYDBRIDIZATION CASE 111

8.5. CONSIDERATIONS 112

9. FUTURE PROSPECTS 114

9.1. EVALUATION OF THE FEASIBILITY USING EXPERIMENTAL TECHNOLOGIES 116

10. GRAVIMETRIC INDEX COMPARISON BETWEEN LOHC AND LH_2 117

11. CONCLUSIONS 118

BIBLIOGRAPHY 120

ABSTRACT

Today, global warming has reached alarming levels and will only worsen if greenhouse gas emissions are not reduced. Of all types of transport, aviation is the most polluting. A solution for decarbonizing the aerospace industry is represented by hydrogen, thanks to its high gravimetric energy density. However, the main challenge of H_2 is related to its storage. Due to its very low density, H_2 is not competitive in the transport sector. Thus, to increase its density, technologies such as compressed hydrogen, liquified hydrogen, liquid organic hydrogen carriers and metal hydrides are used. The fuel cell system is another key component in the decarbonization scenarios. Indeed, thanks to it, electrical power is generated without pollutant emissions.

The aim of this thesis is to eliminate CO_2 emissions from aircrafts. For this reason, the "ATR-72 600" propulsion will be made completely electric thanks to the use of an SOFC system. The fuel will be hydrogen stored in "perhydro-dibenzyltoluene", a well-known LOHC technology.

The various storage technologies will be discussed in great depth, explaining their properties, dynamic behavior and hydrogen release processes. Then, the characteristics and dynamic behavior of the fuel cell mentioned above will be studied. Once the most promising storage and fuel cell will be chosen, they will be coupled and modeled through Aspen Plus. Then the weight of the whole system will be evaluated and a sensitivity analysis, by changing the parameters of the fuel cell, will be carried out to reduce the system weight as much as possible. Finally, a gravimetric index, related to the H_2 storage and releasing system, will be calculated to make a comparison with other commercial H_2 storage systems.

Unfortunately, the all-electric case of an "ATR-72 600" is not feasible, because of the space and weight requirements of the balance of plant components. Moreover, the airflow required for the fuel cell stack and the system cooling, would involve a

large air intake in the fuselage, which would greatly modify the aerodynamics of the aircraft. For this reason, some degree of hybridization must be examined.

LIST OF FIGURES

Figure 1 Type IV standard pressure vessel [2] 18

Figure 2 Cryogenic hydrogen tank [3].....20

Figure 3 Scheme of LOHC concept [5] 22

Figure 4 Scheme of metal hydride storage technology [7] 24

Figure 5 Change of the hydrogen released in the function of the temperature variation [9].....30

Figure 6 Delay in the reactor response [10].....31

Figure 7 Change of the hydrogen released as a function of the pressure reactor variation [9].....31

Figure 8 Change of the hydrogen released as a function of the LOHC feed mass flow variation [9] 32

Figure 9 Reduction of hydrogen capacity due to cyclic dehydrogenation[15].....36

Figure 10 Hydrogenation and dehydrogenation stages of DBT [24].....43

Figure 11 Simplified H0-DBT/H18-DBT release cycle [23] 44

Figure 12 Working principle of a PEMFC [28].....46

Figure 13 Dynamic response of the FC voltage at different air humidity values [30].....48

Figure 14 Voltage variation due to current change [31].....48

Figure 15 Working principle of a SOFC [32].....49

Figure 16 SOFC dynamic response due to a load variation [33].....51

Figure 17 Dynamic response due to R_{load} change [34].....52

Figure 18 Hydrogen release unit.....55
Figure 19 SOFC system.....56
Figure 20 LOHC storage and SOFC system.....64
Figure 21 Shape of the LOHC tank.....67
Figure 22 Shape of the tank for the determination of $\boldsymbol{\varphi 0}$.....68
Figure 23 Horizontal tube reactor scheme [23].....72
Figure 24 Map of the dehydrogenation grade as a function of the LHSV [23].....73
Figure 25 Weight contribution in terms of percentage of each component with respect to the entire system weight.....81
Figure 26 Comparison between the conventional and all-electric MTOW.....82
Figure 27 Evolution of the H_2 flow entering and exiting the anode, and of the gas temperature exiting the catalytic burner.....86
Figure 28 Evolution of the H2 release, SOFC and global system as a function of the FU.....87
Figure 29 Percentage contribution of each component in terms of weight with a FU=0.85.....89
Figure 30 Heat exchangers weight reduction as a function of the pressurization .91
Figure 31 Weight impact of each component on the overall system for a pressurization p=1.95 bar.....93
Figure 32 Impact of each component on the overall system for a pressure drop in the heat exchangers of 0.34 bar.....95
Figure 33 Weight reduction for each sensitivity analysis carried out.....97
Figure 34 Comparison between the conventional and the best configuration of the all-electric MTOW.....98

Figure 35 Weight impact of each component in percentage terms on the overall system for 80% of hybridization.....101
Figure 36 Comparison between the conventional and the MTOW for a HD = 80% 102
Figure 37 Weight impact of each component in percentage terms on the overall system for 60% of hybridization.....104
Figure 38 Comparison between the conventional and the MTOW for a HD = 60% 106
Figure 39 Weight impact of each component in percentage terms on the overall system for 40% of hybridization.....108
Figure 40 Comparison between the conventional and the MTOW for an HD = 40% 109
Figure 41 Weight impact of each component in percentage terms on the overall system for 20% of hybridization.....111
Figure 42 Comparison between the conventional and the MTOW for an HD = 20% 112
Figure 43 Evolution of the overall system and MTOW weight as a function of the HD.....113
Figure 44 Weight impact of each component in percentage terms on the overall system using sperimental technology 115
Figure 45 Comparison between the conventional and the MTOW for an HD = 20% using experimental technologies 116

LIST OF TABLES

Table 1 Standard pressure vessel types [2] 18
Table 2 Summary of dehydrogenation conditions according to [5] 28
Table 3 Summary of dehydrogenation conditions according to [8] 29
Table 4 Variation of dehydrogenation conditions at different $LiBH_4$ loading 36
Table 5 Properties of doped $LiBH_4$ [16] 37
Table 6 Variation of dehydrogenation conditions of different MgH_2 loading in CMK-3 [18] 38
Table 7 Power required by the ATR-72 600 65
Table 8 Amount of H18-DBT and H_2 needed to produce 3.7 MW 65
Table 9 H18-DBT dimensions 68
Table 10 Input data for the weight calculation of H18-DBT/H0-DBT in the all-electric case 72
Table 11 Weight and volume contribution of the LOHC tanks in the all-electric case 72
Table 12 Input for reactor weight evaluation in the all-electric case 74
Table 13 Weight of the reactor for the all-electric case 75
Table 14 Input for evaluation of separator gas capacity in the all-electric case 76
Table 15 Input needed for plate heat exchanger weight evaluation in the all-electric case 79
Table 16 Weight and volume of plate heat exchangers for the all-electric case 79
Table 17 Weight and volume of each system in the all-electric case 80
Table 18 Variation of the mass flow rates, stored masses and exhaust gas temperature of the catalytic burner as a function of the FU 85
Table 19 Weight of each component as a function of the FU 86
Table 20 Weight of each subsystem and of the global system 87
Table 21 Weight and percentage contribution on the overall system of H18-DBT stored and heat exchangers 88
Table 22 Gravimetric index of H_2 storage system 89

Table 23 Compressor and heat exchangers weight reduction as a function of the pressurization 90
Table 24 Weight of each subsystem and of the overall system as a function of the pressurization 92
Table 25 Impact decrease on the overall system of the heat exchangers as a function of the pressurization 92
Table 26 Grvimetric index of the H_2 storage system for different pressurizations 93
Table 27 Weight reduction of the heat exchangers for different pressure drops ... 94
Table 28 Impact reduction of the heat exchangers on the overall system for different pressure drops 94
Table 29 Weight of each subsystem and of the overall system as a function of the pressure drop in the heat exchangers 95
Table 30 Gravimetric index of the H_2 storage system for different pressure drop in the heat exchangers 96
Table 31 Comparison between the configuration of each sensitivity analysis 96
Table 32 H18-DBT and H_2 stored and mass flow rate for 80% of hybridization .. 99
Table 33 Weight of each component of the H_2 release system for 80% of hybridization 100
Table 34 Weight of each component of the SOFC system for 80% of hybridization 100
Table 35 Weight of each subsystem and of the overall system for 80% of hybridization 100
Table 36 H18-DBT and H_2 stored and mass flow rate for 60% of hybridization 103
Table 37 Weight of each component of the H_2 release system for 60% of hybridization 103
Table 38 Weight of each component of the SOFC system for 60% of hybridization 103
Table 39 Weight of each subsystem and of the overall system for 60% of hybridization 104
Table 40 H18-DBT and H_2 stored and mass flow rate for 40% of hybridization 106
Table 41 Weight of each component of the H_2 release system for 40% of hybridization 107

Table 42 Weight of each component of the SOFC system for 40% of hybridization 107
Table 43 Weight of each subsystem and of the overall system for 40% of hybridization 107
Table 44 H18-DBT and H_2 stored and mass flow rate for 20% of hybridization 109
Table 45 Weight of each component of the H_2 release system for 20% of hybridization 110
Table 46 Weight of each component of the SOFC system for 20% of hybridization 110
Table 47 Weight of each subsystem and of the overall system for 20% of hybridization 110
Table 48 Weight of the overall system and of the MTOW as a function of the HD 112
Table 49 Comparison in terms of weight between commercial and future technology 114

ACRONYMS

A/V	area to volume ratio
AC	activated carbon
ASR	area specific resistance
BOP	balance of plant
CcH_2	cryogenic compressed hydrogen
CH_2	compressed hydrogen
DoD	degree of dehydrogenation
FCEV	fuel cell electric vehicle
FU	fuel utilization
H0-BT	benzyltoluene
H0-DBT	dibenzyltoluene
H0-NEC	N-ethylcarbazole
H12-BT	perhydro-benzyltoluene
H12-NEC	perhydro-N-ethylcarbazole
H18-DBT	perhydro-dibenzyltoluene
HD	hybridization degree
HSAG	high surface area graphite
HT-PEMFC	high temperature-proton exchange membrane fuel cell

LH_2	liquified hydrogen
LHSV	liquid hourly space velocity
LOHC	liquid organic hydrogen carrier
LT-PEMFC	low temperature-proton exchange membrane fuel cell
MCH	methylcyclohexane
MH	metal hydride
MI	melt infiltration
MOF	metal organic framework
MTOW	maximum take off weight
OCV	open circuit voltage
PEMFC	proton exchange membrane fuel cell
SOFC	solid oxide fuel cell
TPI	toxic potential indicator
TRL	technology readiness level

1. INTRODUCTION

To date, most industries and means of transportation, such as trucks, ships, cars and aircrafts, use fossil fuels. This has resulted and will result in a continued increase in the amount of CO_2 in the atmosphere. For this reason, today there are many objectives concerning the decarbonization of both the energy system and transport. To meet the decarbonization target, renewable energies must be used. In Europe there are two targets about the decarbonization in the aviation field: the 55% reduction of the greenhouse gases by 2030 and the zero net emissions by 2050 [1]. To achieve these targets, hydrogen represents the main actor. Indeed, the coupling between hydrogen and fuel cell allow to produce power with zero emissions.

Using H_2, the most important parameter in terms of storage is the density. Nowadays, different methods of hydrogen storage are available and allow to increase its density. They can be mainly classified as physical-based and chemical-based methods. In this thesis, the second option has been studied and in particular, the storage in form of liquid organic compound has been investigated.

About fuel cells, there are different technologies depending on the reactants used and the working temperature. In the transport sector, where high performance and versatility are required, low-temperature PEMFC and high-temperature SOFC are the most suitable for this role.

Once the best LOHC technology and the best fuel cell type will be found, they will be put together to represent a possible solution to decarbonization.

2. H_2 STORAGE TECHNOLOGIES

Nowadays, several technologies, commercialized or still under research, are able to store hydrogen. Among them, the most relevant for the storage of hydrogen on board aircraft are the following:

- Compressed hydrogen (CH_2);
- Liquified hydrogen (LH_2);
- Cryocompressed hydrogen (CcH_2);
- Metal Organic Frameworks (MOFs);
- Metal Hydrides (MH);
- Liquid Organic Hydrogen Carrier (LOHC);
- Ammonia (NH_3).

However, only CH_2, LH_2, MH and LOHC will be considered in the following analysis.

2.1. COMPRESSED HYDROGEN

Compressed hydrogen is the most well-known technology in the market. Indeed, there are already commercialized Fuel Cell Electric Vehicle (FCEV), such as Toyota Mirai, Hyundai Nexo, Hyundai ix35, and others, which are using compressed H_2 as storage.

Hydrogen is compressed to increase its density, reaching values of 57.47 kg/m^3 for a pressure equal to 700 bar under near ambient temperature. Because of the nature of the hydrogen, generally, the last generation tanks have to be coated with three layers: a high-density polymer in order to avoid embrittlement, a graphite layer and a glass fibers layer.

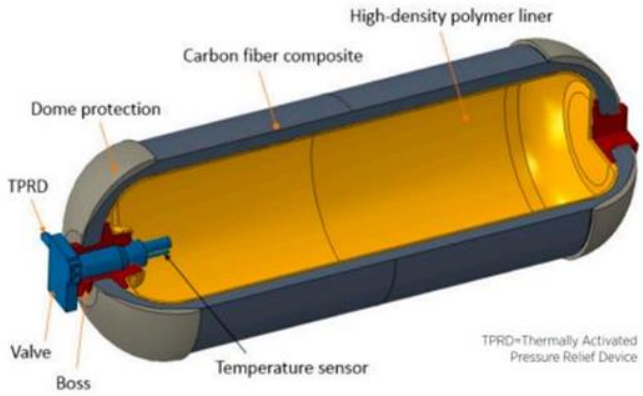

Figure 1 Type IV standard pressure vessel [2]

Over the years, the tank has been continuously studied and improved, to achieve better and better performances. So far, four types of tanks are developed, and they are listed in Table 1:

Type	Materials	Typical Pressure [bar]	Gravimetric Density [wt%]
I	All-metal construction	300	1.7
II	Mostly metal, composite overwrap in the hoop direction	200	2.1
III	Metal liner, full composites overwrap	700	4.2
IV	All-composites construction	700	5.7

Table 1 Standard pressure vessel types [2]

When the hydrogen is compressed, it releases heat. For this reason, it is cooled down before being compressed avoiding a too high increase in temperature inside the tank. Apart from this procedure, once the storage is filled and ready to be used, no more thermal management is required [2].

2.1.1. ADVANTAGES AND DISADVANTAGES OF CH_2

Concerning the advantages of this technology, they are:

- high purity of H_2, avoiding the catalyst poisoning;
- easiest way to store H_2, just a compressor is needed, avoiding chemical reactions or cryogenic cycles;
- fast hydrogenation/dehydrogenation, to response without significant delay to load variation.

On the other hand, the disadvantages are:

- high storage pressure which leads to thicker and havier tank walls to handle the stresses;
- low volumetric density, thus high volume requiring space are needed to store sufficient hydrogen;
- high TRL, meaning few possibilities of improvement.

2.2. LIQUIFIED HYDROGEN

Liquefaction is the most studied process for hydrogen storage in the field of aviation. The temperature needed to liquefy H_2 is equal to 20 K at atmospheric pressure. Thanks to these thermodynamic conditions, it is possible to achieve a volumetric density equal to 71 kg/m^3.

Thus, the main challenge of LH_2 is to avoid or, at least, minimize the boil-off. Boil-off is related to the evaporation of liquid H_2 due to an increase in temperature, leading to a decrease in volumetric density. For this reason, in most cases, the storage is made up of a double coating whose inside is empty to prevent the passage of heat by conduction or convection.

Moreover, protective panels with low heat emission based on plastic and aluminum are installed between the walls of the container to prevent heat irradiation.

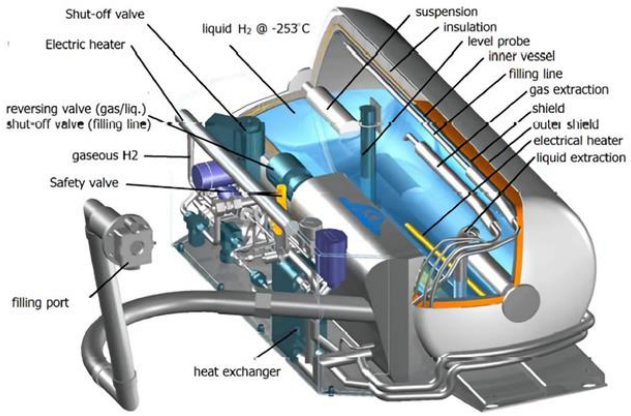

Figure 2 Cryogenic hydrogen tank [3]

The other main challenges of storing hydrogen in liquid form are linked to the geometrical design and thermal design. From the geometrical point of view, it is important to find a shape that ensures a low Area to Volume (A/V) ratio to minimize the boil-off.

Simultaneously, the thermal insulation has to be designed in order to minimize the heat transfer from the external ambient, in order to avoid a too high increase in temperature inside the tank, which leads to the evaporation of the liquid H_2 [4].

2.2.1. ADVANTAGES AND DISADVANTAGES OF LH2

The advantages of liquified hydrogen are:

- high volumetric density, requiring not so much space where storing the tank;
- high hydrogen purity;

- near ambient pressure in the tank, avoiding significant stresses that leads to have thick and heavy tank wall.

Instead, the disadvantages are:

- cryogenic temperature thus a big expenditure of energy is needed;
- evaporation losses requiring to vent the hydrogen and thus loosing it;
- high TRL.

Focusing on the weight, it could be a problem depending on the tank wall and insulation material used.

2.3. LIQUID ORGANIC HYDROGEN CARRIER

Liquid Organic Hydrogen Carriers (LOHCs) offer a promising way to store hydrogen using chemical reactions, mostly under ambient conditions. In this technology, the hydrogen is bounded to the LOHC which shows properties similar to diesel or gasoline.

LOHCs, in particular, are compounds that could be in liquid form or low-melting solid. The most important characteristic of these substances is the possibility of being reversibly hydrogenated and dehydrogenated at high temperatures thanks to the presence of a catalyst. Depending on the type and amount of catalyst used, the temperature needed for dehydrogenation or hydrogenation may be decreased, favoring the reaction. Another key aspect is related to the initial structure of the LOHC. Indeed, it remains the same despite the stored hydrogen being released. For instance, fossil fuels are combusted entirely, without the possibility of being recharged [5].

Concerning the hydrogen storage capacity, LOHCs ensure a gravimetric density in the range of 6-8 wt%, without the need for cryogenic temperature or high-pressure tanks, since the hydrogen is stored under ambient conditions [6].

In this way, hydrogen can be easily stored also for a long-term period, without experiencing the boil-off phenomenon, or it can be transported over long distances.

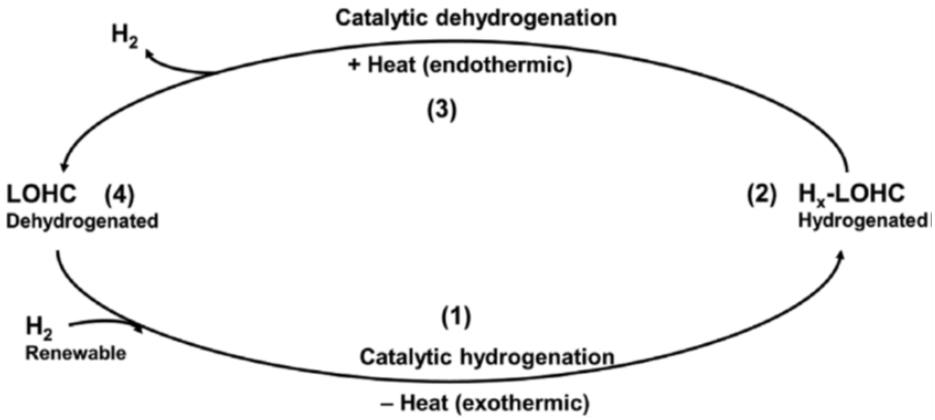

Figure 3 Scheme of LOHC concept [5]

As can be seen in Figure 3, the LOHC concept consists of four stages:

1. catalytic hydrogenation, in which heat has to be provided to a reactor to allow the LOHC to absorb H_2 (exothermic reaction);
2. the hydrogenated LOHC is stored or directly transported to the final user;
3. catalytic dehydrogenation, where the H_2 is released with consequent release of heat (endothermic reaction);
4. the dehydrogenated LOHC is stored and it can be subjected to a new hydrogenation process.

2.3.1. ADVANTAGES AND DISADVANTAGES OF LOHCs

The advantages that characterize LOHCs are:

- reversibility without excessively compromising the initial capacity, reducing the cost of the technology;

- good gravimetric density, thus a high amount of hydrogen can be stored without having too large weight ;
- storage at ambient conditions, avoiding evaporation losses or thick and heavy tank wall or insulation material;
- low TRL, meaning a high potential for improvement.

On the contrary, the disadvantages are:

- need of auxiliary components for dehydrogenation, such as the reactor increasing the weight of the system;
- high temperature needed for releasing hydrogen, thus expenditure of energy is required;
- noble catalyst necessary for reaching reasonable temperature, that could be poisoned because of impurites.

2.4. METAL HYDRIDES

Hydrogen can be stored by a chemical reaction with an alloy that absorbs it forming a metal hydride (MH). Indeed, the metal hydrides are compounds of one or more cations, represented by the metals, and one or more anions, represented by the hydride.

This technology's working principle consists of absorbing hydrogen at low pressure and low temperature, forming a hydride and releasing heat (Q), according to the following reaction:

$$M + \frac{x}{2} H_2 \leftrightarrow MH_x + Q \quad (1)$$

Then, the hydrogen is released when heating the hydride to a specific temperature and pressure. The schematic procedure can be seen in Figure 4.

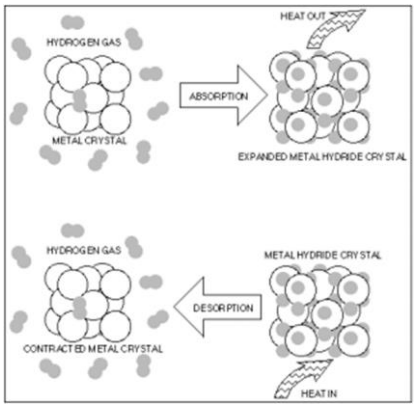

Figure 4 Scheme of metal hydride storage technology [7]

2.4.1. ADVANTAGES AND DISADVANTAGES OF METAL HYDRIDES

The advantages of metal hydrides are:

- safety, since heat is needed to release hydrogen, avoiding accidental leakages;
- high energy density, thus small quantity are needed to provide high energy;
- low TRL.

In contrast, the disadvantages are:

- life cycle, because the charging and discharging leads to the degradation of the material, with consequent decrease of the storage capacity requiring the change of the MH frequently;
- weight, because the materials are heavy, making critical to meet the weight requirement;
- release of H_2 in steps, thus the release is slow and it could not follow the load variation.

3. STORAGE TECHNOLOGIES CONSIDERED

Once the typical characteristics of each technology are evaluated, there will be a further study only on the LOHC ad MH technologies. This is due mainly to the fact that a key point of this thesis is to study low TRL hydrogen storage technologies, because they are characterized by a strong potential for improvement. In the next chapters, thermodynamic properties, dynamic characteristics and storage conditions of the LOHCs and MHs will be analyzed.

3.1. LOHC MATERIALS CONSIDERED

Liquid Organic Hydrogen Carriers are categorized in:

- homocyclic compounds having identical C-C bonds in the dorsal framework;
- heterocyclic compounds with C-N bonds or C-O bonds.

Homocyclic compounds are characterized by high chemical stability, which complicates the desorption of hydrogen, low mobility, high biodegradability and, more or less, low prices. For heterocyclic compounds, with heteroatoms such as N or O that destabilize nearby C-H bonds, a lower dehydrogenation temperature is achieved. In addition, they are too expensive to be used commercially [6].

In this paragraph the LOHCs considered belong to:

- cyclic hydrocarbons such as benzene/cyclohexane, toluene/methylcyclohexane, naphthalene/decalin, biphenyl/bicyclohexyl, dibenzyltoluene (H0-DBT)/perhydro-dibenzyltoluene (H18-DBT) and benzyltoluene (H0-BT)/perhydro-benzyltoluene (H12-BT) ;

- carbazole derivatives such as N-ethylcarbazole (H0-NEC)/ perhydro-N-ethylcarbazole (H12-NEC).

Cyclic hydrocarbons, in most cases, exhibit hydrogen storage capacities ranging from 6 to 8 wt% and hydrogenation and dehydrogenation heat ranging from 62 to 72 kJ/mol_{H_2} [5].

The main parameters that will be considered are storage capacity, dehydrogenation temperature and pressure, toxicity and stability.

3.1.1. DEHYDROGENATION CONDITIONS OF LOHCs

The dehydrogenation process is dependent on the type of reactor, in which the chemical reactions occur, and on the thermodynamic conditions within the reactor itself. Indeed, a drawback of this storage technology is the high temperature and/or high pressure required to desorb hydrogen. So, catalysts are used to decrease the dehydrogenation temperature and to promote the desorption of H_2. The catalyst mostly used are Platinum (Pt), Nickel (Ni) or Molybdenum (Mo) [5].

Considering Decalin, which is the hydrogenated form of naphthalene, it has a hydrogen storage capacity of 7.4 wt% and an energy density of 2.2 kWh/L. Naphthalene is characterized by a high toxicity potential indicator (TPI) and it is likely carcinogenic. On the other hand, decalin shows a quite small TPI in comparison with naphthalene. A major disadvantage in terms of storage is that naphthalene is solid under ambient conditions. Therefore, to have it in liquid form at ambient temperature, toluene as a solvent has to be added, which consequences are the need for a purification stage to purify the hydrogen released and a decrease in the capacity and energy density. Normally, a catalyst made of platinum on a carbon support is used to reduce the dehydrogenation temperature. By using that catalyst is possible to release the hydrogen in 150 min, at 280 °C. Keeping constant the dehydrogenation temperature, by adding rhenium (Re) to the catalyst, it is possible to decrease the required time to 120 min [8].

Instead, according to reference [5], the dehydrogenation of decalin is easier than the dehydrogenation of MCH and it is possible to almost obtain the entire release of stored hydrogen at 280 °C within 1 hour, using a platinum (Pt) and rhodium (Rh) composite catalyst supported on granular activated carbon (AC) in superheated liquid-film states.

N-ethylcarbazole is the dehydrogenated form of perhydro-N-ethylcarbazole. Its storage capacity is equal to 5.8 wt% and the energy density is equal to 2.5 kWh/L. As decalin, N-ethylcarbazole is solid under ambient conditions. Indeed, its melting temperature is equal to 69 °C [5]. To get rid of this problem, hydrogenation is limited to 90% avoiding the addition of a solvent and a purification stage [8] or a longer alkyl chain substitute [5]. The consequence of limited hydrogenation is the reduction of the storage capacity to 5.2 wt% and of the energy density to 2.25 kWh/L. The TPI is equal to 5.1 TPI/mg for N-ethylcarbazole, while for the hydrogenated form this data is not known. To reduce the dehydrogenation temperature, heterogenic catalysts made of palladium (Pd) and ruthenium (Ru) are supported by aluminum oxide (Al_2O_3). Thanks to the catalyst, the entire amount of stored hydrogen is released at 270°C in 25 min or 180°C in 250 min [8]. Otherwise, 98% hydrogen release in 1.5 hours at 250°C can be achieved through the use of the Ni-NiCrO catalyst and benzene as a solvent [5].

Methylcyclohexane is the hydrogenated form of toluene. It is characterized by a storage capacity of 6.2 wt% and an energy density of 1.6 kWh/L, but it is set a limit in the dehydrogenation of 95% leading to achieving a storage capacity of 5.9 wt% and an energy density of 1.5 kWh/L. Toluene is liquid at ambient conditions, has a quite high toxicity potential indicator and is flammable, while MCH has a lower TPI and is dangerous to the environment. Focusing on the dehydrogenation process, no information about time is available, while a temperature in the range of 250-450 °C is needed. In particular, a catalyst made of platinum (Pt) or nickel (Ni) supported on Al_2O_3 is used. With a temperature starting from 350 to 450 °C is possible to release between 50 and 92% of the hydrogen stored. To increase the hydrogen yield to a maximum value of 95%, a catalyst made of potassium and

platinum supported on aluminum oxide and a temperature equal to 320 °C are necessary [8].

Dibenzyltoluene is a substance already used in industries as heat transfer oil. It is the dehydrogenated form of perhydro-dibenzyltoluene. This LOHC is capable of storing 6.2 wt% of hydrogen, achieving an energy density of 1.9 kWh/L. Dibenzyltoluene is liquid under ambient conditions and it remains liquid during all the process of dehydrogenation avoiding the need for a purification stage of the released hydrogen. Considering the TPI, dibenzyltoluene has a value equal to 13.8 TPI/mg while for the H18-DBT this data is not known. The conditions for dehydrogenation require a palladium (Pd) and ruthenium (Ru) catalyst supported by carbon. In this way, it is possible to obtain the release of the 97% of stored hydrogen in 120 min at 310°C. To obtain full desorption of H_2, temperatures higher than 310 °C are necessary. It is obvious that also lower temperatures can be applied, but consequently, a lower percentage of hydrogen will be released. For instance, at 270 °C only 40% of the stored hydrogen is released within 2 h [8].

Benzyltoluene is the dehydrogenated form of perhydro-benzyltoluene, which is characterized by a hydrogen storage capacity of 6.2 wt%. For dehydrogenation, a platinum catalyst on a carbon support is used. So, to obtain the release of more than 95% within 210 minutes using the catalyst previously mentioned, a temperature equal to 270 °C is needed. Further studies on increasing the dehydrogenation temperature to decrease the release time have not been studied as the boiling temperature of H12-BT is 270 °C [5].

The data abovementioned are summarized in Table 2 and Table 3:

LOHC-	LOHC+	H2 capacity [wt%]	Enthalpy of hydrogenation/ dehydrogenation [kWh/kg H2]	Dehydrogenation time [min]	Dehydrogenation temp [°C]
Benzene	Cyclohexane	7.2	9.528		375
Toluene	Methylcyclohexane	6.2	9.486		200-320
Naphtalene	Decalin	7.3	9.222	60	280
H0-DBT	H18-DBT	6.2	8.61-9.86	210	290
H0-BT	H12-BT	6.2	8.61-9.86	210	270
H0-NEC	H12-NEC	5.8	7.361	90	250

Table 2 Summary of dehydrogenation conditions according to [5]

LOHC-	LOHC+	H2 capacity [wt%]	Energy density [kWh/L]	Enthalpy of hydrogenation/ dehydrogenation [kWh/kg H2]	Dehydrogenation time [min]	Dehydrogenation temp [°C]
Toluene	Methylcyclohexane	6.2	1.6	9.486		250-450
Naphtalene	Decalin	7.4	2.2	9.208	120	280
H0-DBT	H18-DBT	6.2	1.9	9.083	120	310
H0-NEC	H12-NEC	5.8	2.5	7.389	25	270

Table 3 Summary of dehydrogenation conditions according to [8]

3.1.2. DYNAMIC BEHAVIOR OF LOHCs DEHYDROGENATION

Talking about the dynamic behavior of LOHCs, the rate of hydrogen production and thus to the mass flow rate are examined. In order to modify the hydrogen release, is possible to choose another catalyst, but once changed it is not anymore possible to increase or decrease the desorption as a function of the load variation. The second option is to change some parameters related to the reactor, allowing to vary the speed of release of hydrogen according to the load variation.

The parameters that could be changed are:

- reactor temperature;
- reactor pressure;
- LOHC feed mass flow.

In general, under dynamic applications in which the load variation is fast and hence should the release of hydrogen be as well, the adjustment of the reactor temperature or reactor pressure is preferred. Indeed, a change in LOHC temperature or reactor pressure allows a much more rapid change in hydrogen release than a change in the LOHC feed mass flow as it will be seen in the next sentences.

Starting from the temperature variation, a reduction from 330 to 320 °C is considered. Concerning the other parameters of the reactor, a pressure equal to 3 bar and a LOHC mass flow rate of 9 kg/h are set [9].

As can be seen in Figure 5, the temperature change takes more or less 20 minutes, which evolution is represented by the green line, followed almost instantly by a reduction in the release of hydrogen, which evolution is represented by the blue line.

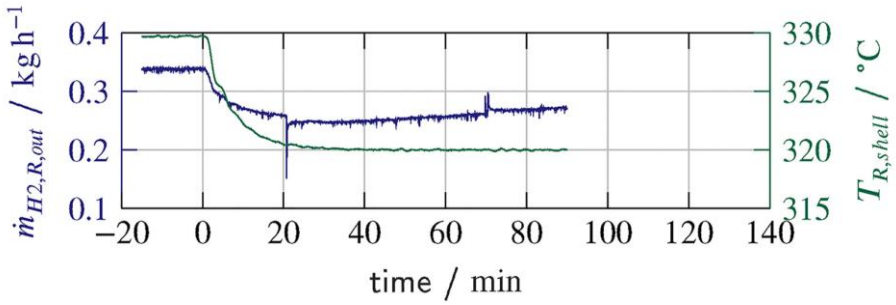

Figure 5 Change of the hydrogen released in the function of the temperature variation [9]

Since dehydrogenation is an endothermic process, the lower the temperature the lower the flow rate of hydrogen produced.

While acting on the temperature may seem interesting, a major drawback must be taken into account: the heating or cooling of the reactor. Indeed, for example, considering to increase the temperature of the LOHC, is simple because the mass flow rates of the latter are not too high. On the contrary, it is much harder to heat a reactor due to its enormous thermal inertia, which leads to a significant delay in the response to load variation. A possibility to decrease the time needed for heating the reactor, is to introduce electric resistances directly inside the reactor to the detriment of efficiency [10]. The delay due to heating the reactor can be seen in Figure 6.

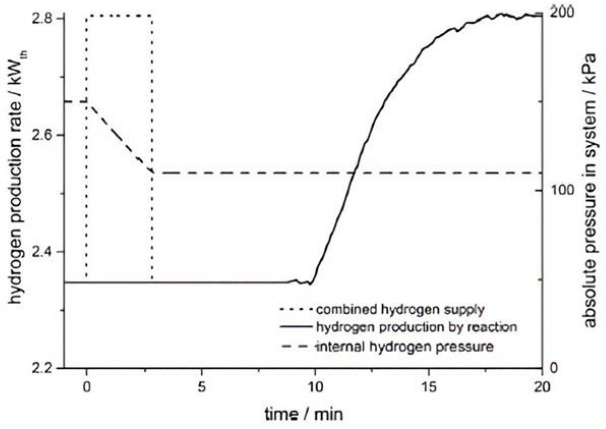

Figure 6 Delay in the reactor response [10]

Then, it is evaluated the dynamic response due to a change in the pressure reactor. In this case, the pressure is increased from 2 to 3 bar, maintaining a temperature of 330 °C and a LOHC mass flow rate equal to 6 kg/h [9].

The variation in the hydrogen release as a function of the reactor pressure can be analyzed in Figure 7.

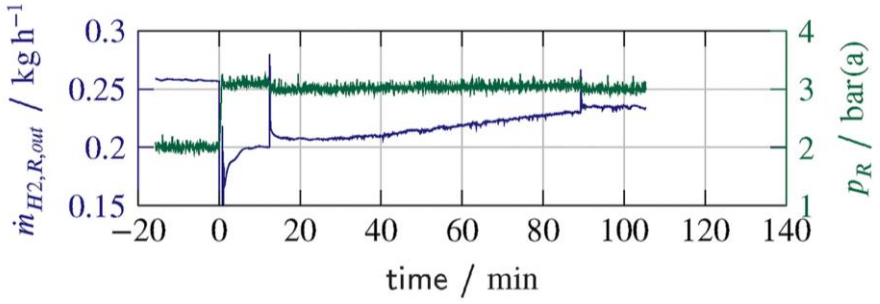

Figure 7 Change of the hydrogen released as a function of the pressure reactor variation [9]

A change in the reactor pressure (green line) ensures the fastest change in the desorption of hydrogen (blue line). Indeed, as can be seen in Figure 7, the variation of the reactor pressure is sudden. The time needed to reach the new state takes a few minutes if not seconds. Simultaneously, there is not a delay in the change of the hydrogen released, but it happens in a synchronous manner.

It is possible to notice, both in Figure 5 and Figure 7, that even though the temperature and the pressure remain constant after load variation, the hydrogen release increases reaching a new steady state instead of being constant. This phenomenon can be explained by the fact that a lower temperature and a higher pressure allow a lower LOHC evaporation with a consequent higher liquid-to-gas ratio. The lower amount of LOHC evaporated means to have a higher residence time of the LOHC in the reactor and so a larger release of hydrogen [9].

To obtain the fastest response in terms of desorption of hydrogen, it is recommended that the pressure and temperature within the reactor are adjusted simultaneously.

The last parameter that could be changed is the LOHC feed mass flow. In particular, it will be considered an increase from 6 to 12 kg/h, keeping constant the temperature at 330 °C and the pressure at 3 bar [9]. The results are represented in Figure 8.

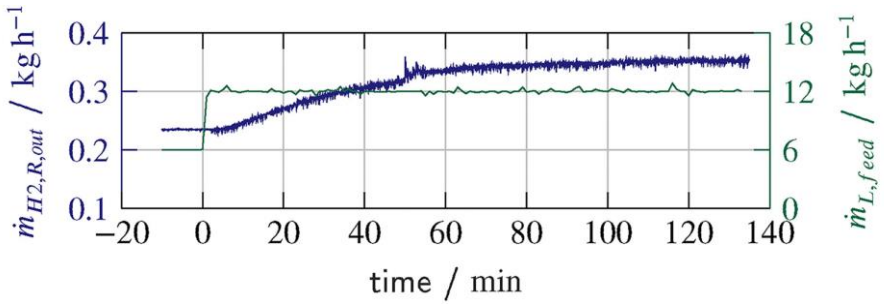

Figure 8 Change of the hydrogen released as a function of the LOHC feed mass flow variation [9]

Looking at Figure 8, is possible to notice the slowness of the process. Indeed, once the LOHC feed mass flow is changed (green line), the release of hydrogen (blue line) takes at least 2 hours to reach the new steady state. Although hydrogen production is increasing significantly, this variation is not justified by time requirements. In addition, to doubling the hydrogenated LOHC flow rate only 49% more hydrogen release is achieved [9]. This could be explained by the fact that increasing the mass flow rate of LOHC, leads to a decrease in the residence time in the reactor and so a lower efficiency in the release of hydrogen.

So, depending on the approach used, the release of hydrogen from LOHCs can be adjusted as a function of the load variation, but as seen in this section, LOHCs are not characterized by very rapid dynamics. For applications characterized by fast dynamics, a buffer tank in which to store compressed H_2 is mandatory. Otherwise, it is impossible to provide the hydrogen needed for satisfying the new demand. Especially a buffer tank, according to [11], is needed during:

- up transients: to provide hydrogen when the dehydrogenation rate is not sufficient to follow the instantaneous demand;
- down transients: to store the hydrogen produced in excess with respect to the quantity demanded;
- heating of the component of the storage system, in case the heat source comes from burning the H_2 itself instead of using another heat source.

3.2. METAL HYDRIDE MATERIALS CONSIDERED

Metal hydrides used for hydrogen storage, normally are “single metal hydrides”. These ones can be categorized in [12]:

- ionic: are also called "saline hydrides" and are made up of most s-block metals[1]. Few examples are Li-Cs and Mg-Ba. It is important to note that the metal-hydrogen bonding of MgH_2 shows a partial covalent behavior;

- covalent: hydrides within p-block metals[2] including also Beryllium (Be), in which there is a covalent bond. They embrace 0D molecular crystals or polymeric 3D networks;

[1] s-block metals: periodic table metals belonging to groups IA and IIA.
[2] p-block metals: periodic table metals belonging to groups from IIA to VIIA.

- interstitial: binary hydrides[3] composed of transition metals, hydrides of lanthanides ($LnH_{n<3}$) and some actinide hydrides. In this case, there is a metallic bond.

In particular, the metal hydrides that will be studied are: lithium hydride (LiH), lithium borohydride ($LiBH_4$), magnesium hydride (MgH_2), sodium alanate ($NaAlH_4$) and sodium borohydride ($NaBH_4$).

3.2.1. MH DEHYDROGENATION CONDITIONS

For metal hydride, in most cases, the dehydrogenation process can be improved by acting on two parameters: temperature e pressure inside the tank. Indeed, high temperature under ambient pressure, high pressure at ambient temperature or both high temperature and high pressure are needed to release hydrogen. The ways to have more favorable conditions for the desorption of hydrogen are the use of catalysts and the so-called nanoconfinement.

Nanoconfinement consists of downsizing the metal hydride in nanoparticles and confining it into nanoporous materials. In this way, it is possible to obtain faster kinetics, in relation to the bulk counterpart, thanks to the shorter diffusion paths as well as the greater surface available for hydrogen chemisorption [13]. Another advantage of nanoconfinement is the improvement of reversibility, indeed it is suppressed particle growth and phase segregation [14].

The main drawback of nanoconfinement is the reduction of the hydrogen storage capacity. As it is fairly easy to understand, having an additional nanoporous structure in which to store the metal hydride, the available space in the storage tank is reduced.

LiH is characterized by a theoretical hydrogen storage capacity of 12.7 wt% [5] and extreme conditions of dehydrogenation. A temperature of 700 °C at ambient pressure or a pressure of 500 bar at ambient temperature is necessary.

[3] Binary hydrides: materials composed by two elements. One is a metal and the other is hydrogen.

So, to have reasonable conditions for the desorption of the H_2, the LiH is nanoconfined into the nanoporosity of high surface area graphite (HSAG). Thanks to the nanoconfinement in HSAG, the dehydrogenation conditions have changed from a temperature of 700 °C to an initial one of 200 °C with the main peak at 340 °C. Making a comparison with pure LiH, the latter requires more than 8 h at 350°C to be entirely dehydrogenated. Apart from these results, other studies were not assessed due to the difficulty in synthesizing LiH at the nanoscale and the highly reactive and air-sensitive nature of LiH and Li itself [13].

$LiBH_4$ shows a hydrogen storage capacity of 18.5 wt%. The dehydrogenation conditions of the pure borohydride need a temperature higher than 400 °C, because of the strong ionic bonding between Li^+ and $[BH_4]^-$ and the other covalent bond between B atom and H atom. Even in this case, $LiBH_4$ is nanoconfined in a scaffold made from an ultrafine porous Fe_3O_4 skeleton wrapped in carbon. Thanks to this scaffold two main positive aspects are obtained. Fe_3O_4 transforms into active species of FeB and Fe_2B during melt infiltration, thus acting as a bidirectional catalyst and the nanoconfinement ensures additional surface interaction with $LiBH_4$ destabilizing itself. Focusing on the dehydrogenation conditions of the nanoconfined MH, they changed a lot. Indeed, through the confinement with different $LiBH_4$ loading, the starting temperature for desorbing hydrogen is 175°C. In particular, three different $LiBH_4$ loadings are considered: 50, 60 and 70%. Because of the lower amount of $LiBH_4$, there is a smaller quantity of H_2 release with respect to the bulk quantity that under a temperature of 350 °C is the 6.5, 5.8 and 4.9 wt% H_2 for 50,60 and 70 wt% $LiBH_4$ respectively. Increasing the temperature of dehydrogenation up to 400 °C the H_2 released is equal to 6.3, 7.8 and 8.7 wt% for 50,60 and 70 wt% $LiBH_4$ respectively [14]. The results are summarized in Table 4.

$LiBH_4$ loading [%]	Dehydrogenation temp[4] [°C]	H_2 released [wt%]
50	350/400	4.9/6.3
60	350/400	5.8/7.8
70	350/400	6.5/8.7

Table 4 Variation of dehydrogenation conditions at different $LiBH_4$ loading

Another way to improve the dehydrogenation process of $LiBH_4$ is the nanoconfinement through an activated charcoal (AC) prepared by melt infiltration (MI). The study, in particular, considers a loading of 35 wt% of $LiBH_4$. Results indicate a minimum temperature of 190°C to begin dehydrogenation, ending at 400°C and reaching a dehydrogenation capacity of 13.6 %. Moreover, to desorb the 9% hydrogen are required 33 minutes and the complete release of the stored hydrogen, which is more or less 10%, takes 1 hour. The reason for not achieving 13.8% capacity may be due to H_2 losses during the evacuation phase. An important aspect to underline is the bad reversibility of metal hydrides.

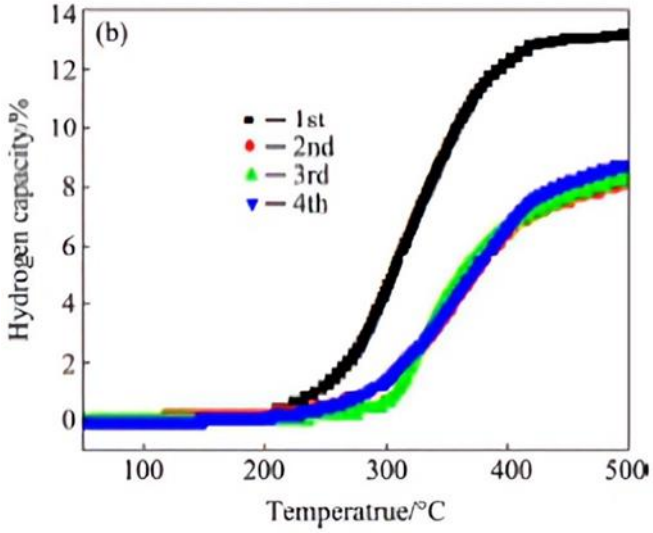

Figure 9 Reduction of hydrogen capacity due to cyclic dehydrogenation[15]

[4] Dehydrogenation temp: temperature needed to release that specific quantity of hydrogen and not the minimum temperature to start the desorption.

As it is possible to see in Figure 9, the reduction of the hydrogen capacity goes from 13.8 wt% for the first cycle to approximately 9 wt% for the second cycle. Therefore, during the first three cycles, the hydrogen capacity of LiBH4 is reduced by 65% [15].

Concerning $LiBH_4$, to change the dehydrogenation conditions to more favorable ones, it can be doped. To evaluate changes, the $LiBH_4$ will be doped considering: $Li_{1+x}B_{1-x}H_4$ where x = 0,0.25,0.5,0.75 [16].

The results obtained are listed in Table 5:

	H2 capacity [wt%]	Dehydrogenation temp [°C]	Desorption enthalpy [kJ/mol]
$LiBH_4$	18.5	385.75	75.75
$Li_{1,25}B_{0,75}H_4$	18.88	269.49	62.38
$Li_{1,5}B_{0,5}H_4$	19.36	261.48	61.46
$Li_{1,75}B_{0,25}H_4$	20.31	134.42	46.854

Table 5 Properties of doped $LiBH_4$ [16]

Thanks to doping not only there is a reduction of 250 °C in the dehydrogenation temperature, but also an increase in the hydrogen storage capacity which are both beneficial.

To understand the reason of these results, it has to be remembered that according to reference [14], the strong covalent bond between B atom and H atom is one of the reasons for the high dehydrogenation temperature. Thanks the doping, there is a lower amount of boron atoms in the lithium borohydride structure, resulting in a weaker hybridization between boron and hydrogen atoms [16].

MgH_2 has a hydrogen storage capacity equal to 7.6 wt% [5][17]. Given that the bulk compound requires a temperature of dehydrogenation higher than 300 °C and a dehydrogenation activation energy of 195.3 ± 10 kJ/mol_{H_2} [17]. Therefore, the nonconfinement of MgH_2 in mesoporous carbon CMK-3, through wet

impregnation method[5], is studied. In particular, the effect of different MgH_2 loadings: 90, 80, 60, 40 and 20 wt% have been evaluated and the results obtained are listed in Table 6.

MgH_2 loading [%]	Dehydrogenation temp [°C]	Max. temp [°C]	H_2 released [wt%]
90	250	358	5.2
80	220	340	4.02
60	180	326	3.7
40	152	300	2.4
20	102	253	1.8

Table 6 Variation of dehydrogenation conditions of different MgH_2 loading in CMK-3 [18]

As it is possible to see in Table 6, considering 90% of MgH_2, the needed initial dehydrogenation temperature is 250 °C, while the bulk material required temperatures higher than 300 °C. In addition, decreasing the MgH_2 load in the CMK-3 scaffold decreases the temperature, which starts the desorption, from 250 °C to 102°C for a 90% and 20% loading of MgH_2 respectively. Simultaneously, decreases the dehydrogenation peak temperature (Max. temp.) of about 100°C. As obvious, decreasing the MgH_2 decreases also the hydrogen storage capacity [18].

Another MH to evaluate is $NaAlH_4$. The dehydrogenation of the sodium alanate is done in two steps:

$$NaAlH_4 = \frac{1}{3}Na_3AlH_6 + \frac{2}{3}Al + H_2 \qquad (2)$$

$$NaAlH_6 = 3NaH + Al + \frac{3}{2}H_2 \qquad (3)$$

The hydrogen capacity of the system is 3.7 wt% for the first step and 1.9 wt% for the second step. Thus, a total hydrogen capacity of 5.6 wt%. Even though the storage capacity is not so high, what is interesting is the dehydrogenation

[5] Wet impregnation is a procedure to load a given porous support, at the solid state, with the metal component, dissolved in a liquid solution [44].

temperature. Indeed, $NaAlH_4$ releases hydrogen at 33 °C and ambient pressure, and Na_3AlH_6 releases it at 130 °C [19].

The last metal hydride that is studied is $NaBH_4$, which has a hydrogen storage capacity of 10.8 wt%. This material is able to release hydrogen via thermolysis[6] or hydrolysis[7], the latter method is the one analyzed. The main advantage of hydrolysis of $NaBH_4$ is the spontaneity of the process that could be accelerated by using catalysts. The process is exothermic, requiring -210 kJ/mol, and it follows the reaction:

$$NaBH_4 + 2H_2O \rightarrow NaBO_2 + 4H_2 \quad (4)$$

The temperature needed to release hydrogen through hydrolysis is quite small, since 25 °C is enough to start the desorption. Despite all these advantages, there is an important drawback represented by the volume of water needed. This is because, in reality, the process happens according to the following reaction, as explained in [20]:

$$NaBH_4 + 4H_2O \rightarrow NaB(OH)_4 + 4H_2 \quad (5)$$

Therefore, instead of having two molar equivalents of water for each mole of $NaBH_4$, four moles are needed. The other negative aspect is due to the rate of reaction. Indeed, because of the low temperature needed, the $NaBH_4$ experiences self-hydrolysis when water is introduced. Thus, to overcome this problem, there is the addition of sodium hydroxide (NaOH) [20].

Another study on $NaBH_4$ is discussed in [21], where considering a 25 wt% loading of sodium borohydride, the hydrogen is released at about 50 °C through hydrolysis. In particular, to release hydrogen at that temperature, an alkaline environment must be guaranteed. To do so, in the solution is added 4 wt% NaOH reaching a pH equal to 14. The rest of the solution is constituted by water.

[6] Thermolysis is a process in which hydrogen is released by heating the storing material.
[7] Hydrolysis is a process where the release of hydrogen is due to a reaction with water.

3.2.2. DYNAMIC BEHAVIOR OF MHs DEHYDROGENATION

As explained in chapter 3.1.2, with dynamic behavior is intended for response in hydrogen release due to a load variation. With respect to LOHCs, the metal hydride, in most cases, is in form of metal powder that is not requiring a reactor to release hydrogen. Indeed, to release hydrogen is enough to act on the temperature and/or pressure inside the storage tank.

In particular, according to [22], the dynamics of the hydrogen release from metal hydride depend mainly on:

- the conditions for supplying and removing heat;
- heat transfer in the MH bed;
- size of the tank.

Considering the heating and cooling conditions, it is important to improve the intensity exchange between the heat-transfer liquid and the heated outer wall of the MH storage. Then, to enhance the heat transfer in the MH bed, the layout feature of the MH tank has to be accurately designed. Concerning the size of the tank, it plays a key role in the dynamics because the larger the storage, the higher will be the thermal inertia.

Depending on the above-mentioned parameters, it is possible to have a mismatch between the dehydrogenation rate and the quantity requested by the instantaneous demand. As explained at the end of chapter 3.1.2, a buffer tank of hydrogen is needed.

3.3. CHOICE OF THE BEST TECHNOLOGY TO BE COUPLED WITH A FUEL CELL SYSTEM

After the evaluation of the properties of the hydrogen storage technologies, the dehydrogenation conditions and the dynamic release of hydrogen, in this chapter only one storage technology will be chosen to be coupled with a fuel cell system.

Starting from the hydrogen storage capacity point of view, in general, metal hydride and especially borohydride show higher storage capacity compared to LOHCs. However, because of the nanoconfinement issue and the need for water to release hydrogen through hydrolysis as regards metal hydrides, the difference between the two storage capacities is no anymore so big.

In this thesis, the coupling of a hydrogen storage technology to a fuel cell system will be studied for aviation applications. In this context, the weight plays a key role and it is decisive for the choice of the storage technology. MHs are composed of one or more metals in the compound, therefore the weight involved is quite large, while for LOHCs only substances liquid at ambient conditions will be considered, which have a much lower weight in comparison with MHs.

Considering the abovementioned observations, LOHC storage technology is chosen to be modeled for coupling with a fuel cell system.

Another reason for choosing LOHCs as storage technology is related to similar properties to already existing fuels such as diesel or gasoline. Thus, LOHCs can use the existing infrastructure used by liquid fossil fuels.

3.3.1. CHOICE OF THE BEST LOHC TECHNOLOGY

Once the LOHC technology has been chosen against MH one, the best substance among the LOHCs will be evaluated.

Concerning the toluene/methylcyclohexane system, it is characterized by a low boiling point (110°C for toluene) of all the components involved, which leads to

the application of considerable condensation and purification stages. In addition, the flashpoint[8] of both substances are below the dehydrogenation temperature (4 °C for toluene), leading to risks from the security point of view. Besides, the density of MCH is equal to 0.77 g/ml, thus not so high [23]. Toluene is flammable and MCH is dangerous to the environment [8].

N-ethylcarbazole because of the presence of nitrogen atom (N) shows different limitations [23]:

- the C-N bounds show thermal lability under catalytic dehydrogenation conditions with consequent N-containing decomposition products that could poison the fuel cells;
- limited availability of N-containing LOHC substances with respect to hydrocarbons.

Moreover, N-ethylcarbazole is solid under ambient temperature [5].

Even naphthalene, as written in chapter 3.1.1 is sold under ambient conditions. In addition, naphthalene is toxic and carcinogenic [5][8].

Benzyltoluene, instead, will not be evaluated because it has similar characteristics to Dibenzyltoluene, but it is more toxic [8].

Concerning perhydro-dibenzyltoluene, it is characterized by a high density equal to 0.92 g/ml, which is one of the highest among the LOHC analyzed. Thanks to the high density, it is possible to store 57 g_{H_2} per liter of H18-DBT. Moreover, H0-DBT is characterized by a high boiling point, which is 390 °C, thus much higher than the dehydrogenation temperature. From a safety point of view, the H0-DBT has a quite high flashpoint (200 °C) and it is not carcinogenic [23].

Therefore, mainly due to the high boiling point, the non-carcinogenicity and the relatively low release of compounds that could be poisonous to the fuel cell, the

[8] Flashpoint: the lowest temperature at which a substance generates enough vapor to form a mixture that may ignite [45].

LOHC technology that is chosen to be coupled to a fuel cell is dibenzyltoluene (H0-DBT).

3.3.1.1. DIBENZYLTOLUENE/PERHYDRO-DIBENZYLTOLUENE

On the system dibenzyltoluene/perhydro-dibenzyltoluene is necessary to make further specifications. Indeed, hydrogenation and dehydrogenation, according to [24], happen in several steps as represented in Figure 10:

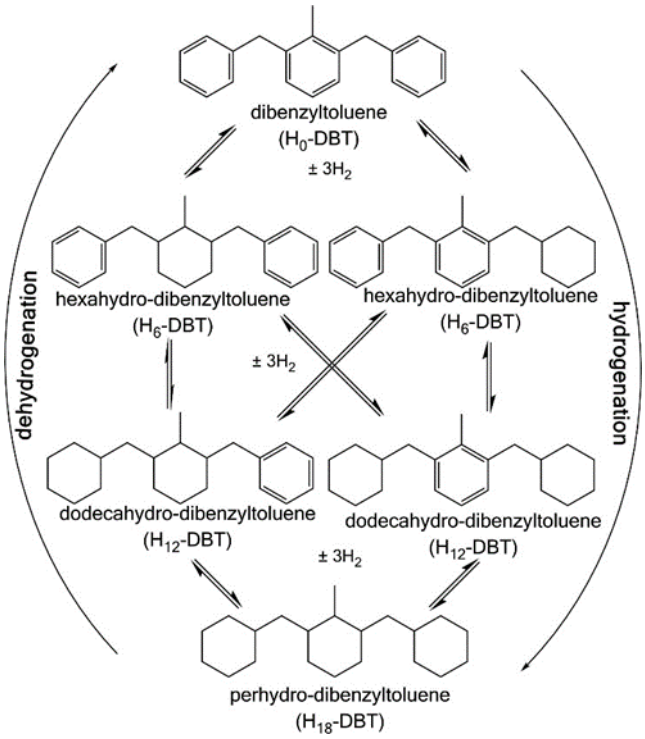

Figure 10 Hydrogenation and dehydrogenation stages of DBT [24]

Nevertheless, in this thesis, the release of hydrogen, as already done in different studies [9][10][23][25], will be modeled as it would happen in a single step. So, the hydrogenation and dehydrogenation cycle takes place not as represented in Figure 10, but as represented in Figure 11.

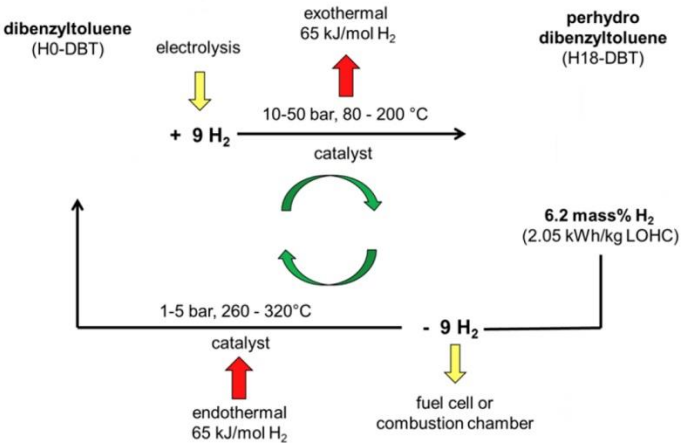

Figure 11 Simplified H0-DBT/H18-DBT release cycle [23]

4. FUEL CELL SYSTEM

The hydrogen produced will not be burned in a combustor, but it will be used in a fuel cell stack. This thesis aims to study a possible solution for the electrification of the aircraft propulsion. Nowadays, there are different types of fuel cells, but the most suitable ones are: Proton Exchange Membrane Fuel Cell (PEMFC) and Solid Oxide Fuel Cell (SOFC) [26].

In the next chapters, the characteristics and the dynamics of each type of cell will be studied, to choose the best FC to be coupled to the LOHC technology.

4.1. PROTON EXCHANGE MEMBRANE FUEL CELL (PEMFC)

PEMFC are low-temperature FC (LT-PEMFC), characterized by fast dynamic, high efficiency and high reliability. The working temperature, in most cases, is around 70 °C, thus precious catalysts like Pt are used.

However, high-temperature PEMFCs (HT-PEMFC) have been developed in recent years that can work at temperatures higher than 120 °C [27].

The working principle of LT-PEMFC can be represented in Figure 12.

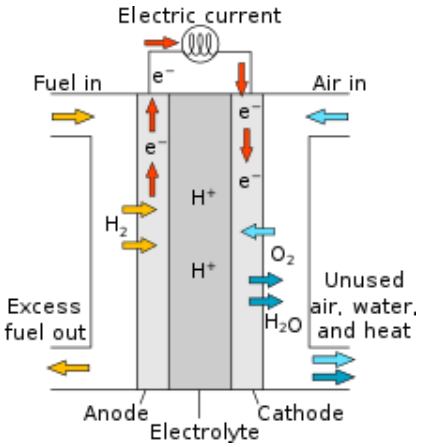

Figure 12 Working principle of a PEMFC [28]

In particular, the anode half reaction, is:

$$2H_2 \rightarrow 4H^+ + 4e^- \quad (6)$$

the cathode half reaction is:

$$O_2 + 4e^- + 4H^+ \rightarrow H_2O \quad (7)$$

Therefore, the complete reaction is:

$$H_2 + \frac{1}{2}O_2 \rightarrow H_2O \quad (8)$$

The state of the art of a PEMFC is:

- electrolyte: composed of Nafion[9], which is Teflon modified by adding a lateral chain in which there is a mobile ion;
- electrode: where there is the catalysis of the electrochemical reaction. It is composed of an active or catalytic layer, characterized by the three-phase boundary[10] and the catalysis, and a support layer that is porous to be a good electronic conductor;

[9] Nafion: name of a polymer used as electrolyte in PEMFC, developed by DuPont (a US chemical company).
[10] The three-phase boundary is composed of: a pore phase to let the substance reach the catalyst, an electronic phase to let pass the electrons and an ionic phase to let pass the ions.

- interconnector: is added to connect in series more than one cell. It has to be a good electronic conductor, dense and easy to machine.

The most important aspects of PEMFC are the following [29]:

- water management: to guarantee a good ionic diffusivity the membrane has to be correctly hydrated. Because of the temperature inside the cell, to avoid the drying of the membrane the water produced at the cathode is recovered and used to humidify the inlet air;
- thermal management: to maintain the cell temperature more or less constant and to avoid overheating an external cooling circuit is needed;
- type of reactants: air or pure oxygen can be supplied to the cathode.

4.1.1. PEMFC DYNAMIC BEHAVIOR

The PEMFC is the best type of FC that can be used for dynamic applications, thanks to the fast kinetic of electrochemical reactions and the low thermal inertia.

The parameters affecting the dynamics of PEMFC are: the temperature of the cell, the membrane humidity, the air stoichiometry and the pressure of the cell [30]. Obviously, to have fast dynamics all these parameters have to be accurately designed and maintained.

For example, to evaluate the dynamic response of a PEMFC a current step increase at different air humidity is analyzed in [30]. The results obtained are represented in Figure 13.

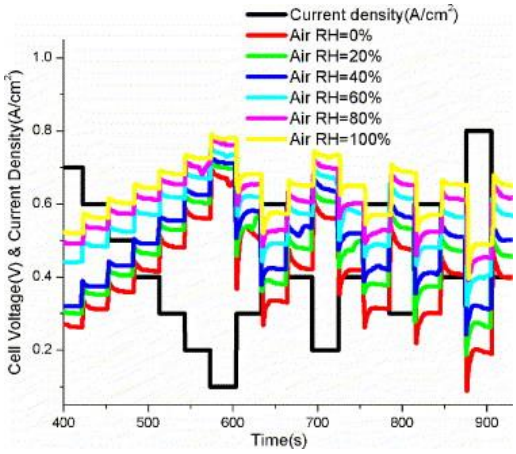

Figure 13 Dynamic response of the FC voltage at different air humidity values [30]

As can be seen in Figure 13, for fully humidified conditions a sudden variation of the cell voltage happens. This allows understanding of how the dynamic response of the cell under precise conditions is very fast. Instead, the PEMFC at a low humidity level, not only does the voltage take longer to reach a new steady state, but it also presents a high voltage undershoot. Concerning the effect of the other parameters on the dynamics of a PEMFC, they are explained in [30].

Another study in which the PEMFC dynamics is studied is [31]. In this paper, to evaluate the dynamic response of a PEMFC, a load variation represented by an increase and decrease of current from 60 A to 100 A at a rate of 20 A/s is chosen. The effects of the load variation can be seen in Figure 14.

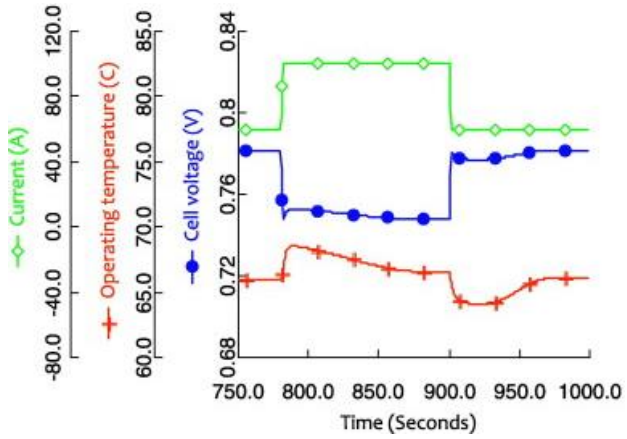

Figure 14 Voltage variation due to current change [31]

As the current increases, there is a synchronous decrease in the cell voltage. This is due to the cell overpotential. At the same time, there is an increase in the stack temperature, because more current is drawn more heat is produced by the reactions. For the temperature, more time is needed because mass transports are slower than electrochemical reactions.

4.2. SOLID OXIDE FUEL CELL (SOFC)

The SOFCs are high-temperature fuel cells that operate in the 700-1000ºC range, thus catalysts like nickel (Ni) can be used.

The working principle of a SOFC is represented in Figure 15.

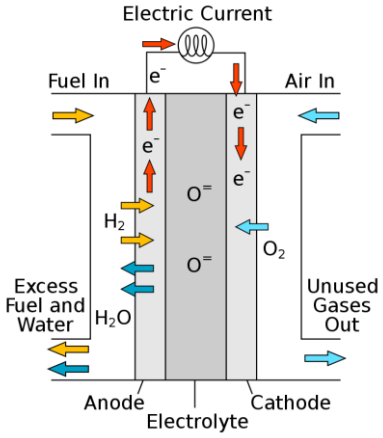

Figure 15 Working principle of a SOFC [32]

In this case, the anode half-reaction is:

$$2H_2 + 2O^{2-} \rightarrow 2H_2O + 4e^- \quad (9)$$

the cathode half-reaction is:

$$O_2 + 4e^- \rightarrow 2O^{2-} \quad (10)$$

Therefore, the complete reaction is:

$$2H_2 + O_2 \rightarrow 2H_2O \quad (11)$$

The state of the art of the components froming the SOFC is reported below:

- electrolyte: made of a ceramic material, normally yttria (Y_2O_3) stabilized zirconia (ZrO_2), that allows good mobility to O^{2-} ions;
- anode: usually made of cermet, which is a ceramic (ZrO_2) – metallic (Ni) composite material. It is porous to ensure good conduction of electrons and ions conductor and from a thermal expansion point of view, it is compatible with the electrolyte material;
- cathode: it has similar characteristics to the anode and it is made of ceramic materials with a perovskite structure (ABO_3). In particular, is made of lanthanum manganite doped with strontium ($(La_{1-x}Sn_x)MnO_3$).
- Interconnector: made of crofer 22 apu, that is stainless steel with 22% of chromium (Cr). It should be a good electronic conductor, chemically stable at high temperatures and with a coefficient of thermal expansion similar to the other components.

There are several advantages due to the high-temperature operation. First of all, there is no need for precious catalysts (nickel is used), since the kinetic is quite fast. Moreover, thanks to high-temperature and the use of Ni as a catalyst, it is possible to oxidize a multitude of molecules (H_2, C_xH_y, $C_xH_yO_k$, NH_3 and others…). Finally, all transport processes are better than the ones in a PEMFC and so a higher electrical efficiency is achieved.

On the other hand, the high-temperature operation leads to having also many drawbacks: long start-up time (few hours), suffering thermal cycles, lower lifetime and the balance of plant (BOP) are more expensive than the case of a PEMFC.

4.2.1. SOFC DYNAMIC BEHAVIOR

The functioning of SOFC depends on the simultaneous transport of charged species, electrochemical reactions, and heat and mass transport.

To study the dynamic response, a load variation represented as a voltage change between 0.8 and 0.93 V is used. The results are shown in Figure 16.

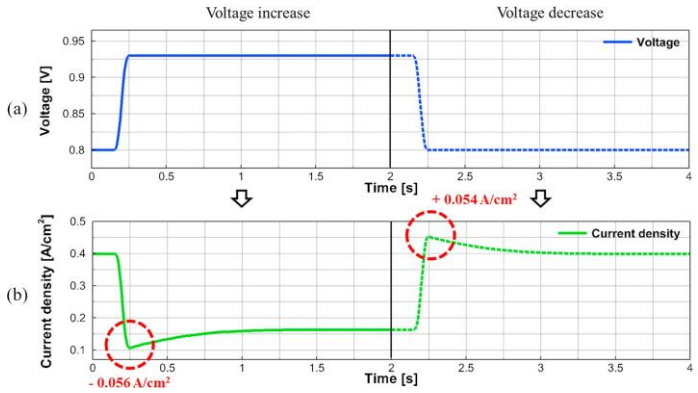

Figure 16 SOFC dynamic response due to a load variation [33]

The voltage increase corresponds to an increase in the current density from 0.4 to 0.16 A/cm^2. As can be seen in Figure 16, the current density change is instantaneous and it takes 2 seconds to reach a new steady state. Therefore, as said also in chapter 4.2.1, the SOFC is characterized by fast kinetics. The real problem of SOFC is related to heat transport, which is much slower than electrochemical reactions. Indeed, according to [33], the temperature takes much more time to reach a new steady state, since the heat produced by the SOFC is transferred through conduction to the incoming gas. Therefore, heat transport is not characterized by a fast response to a new chemical environment when changing the electrical load, leading to thermal stresses.

Another study on the dynamic response of SOFC is presented in [34]. To evaluate the dynamic properties of a SOFC, load resistance step changes from 4 to 2 Ω occurred. In Figure 17 (a) and (b) is possible to see the dynamic response of the voltage and the cell temperature, respectively.

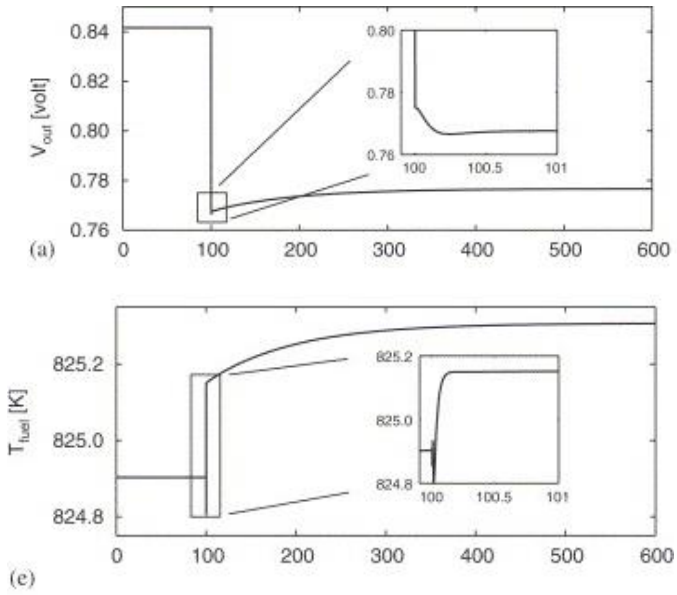

Figure 17 Dynamic response due to R_{load} change [34]

When the load resistance varied, the voltage responds quickly and reaches a new steady state fastly. Focusing on the temperature variation, in Figure 17 (c) it is possible to note the slowness of the response, which takes more than 200 seconds to reach a new operating condition. A change in R_{load} corresponds to a change in the current density that leads to higher heat release. Considering that the heat capacity of the material is large, the heat transport dynamic is slow.

4.3. CHOICE OF THE FUEL CELL TO BE COUPLED WITH THE H18-DBT/H0-DBT SYSTEM

Among the fuel cells analyzed, only one of them will be studied to be coupled with the LOHC technology chosen in the previous chapters.

The fuel cell that will be chosen is the Solid Oxide Fuel Cell, mainly because of its high working temperature. Indeed, thanks to the working temperature of the fuel cell in the range of 700-1000 °C, it is possible to thermal coupling the fuel

cell and the hydrogen storage system by using the exhaust gases for pre-heating the H18-DBT entering the reactor. In the case of PEMFC, this could not have been possible since the temperature of its exhaust gases is, more or less, 70 °C while the one needed for the dehydrogenation is between 300-350 °C. The other reason why the SOFC has been chosen is that it is characterized by higher efficiency. In this way, for the same power output of a PEMFC, the amount of hydrogen to store is reduced and thus the storage system weight is saved.

5. ASPEN MODELING

The software that will be used to study the entire system is Aspen Plus. The entire system will be analyzed under steady-state conditions. The reason is mainly due to the TRL of this technology which is quite low. Therefore, before studying the dynamics of the system, the technical feasibility of the system must be assessed. Since the technical feasibility is evaluated through the weight and volume calculation of each component, it is not necessary to know the component dyanmics.

In the following chapters, firstly the hydrogen release system and then the fuel cell system will be configurated, explaining the function of each block. Once each subsystem will be configurated, the weight of the entire system will be studied.

5.1. H_2 RELEASE SYSTEM CONFIGURATION

In this chapter, the release of the hydrogen stored within the perhydro-dibenzyltoluene is simulated. The weight and volume of each component will be computed in chapter 6.2. The flowsheet of the dehydrogenation process is illustrated in Figure 18.

The main assumptions made in the simulation are:

- steady-state conditions;
- no pressure drops in the reactor.

The thermodynamic property package used in this study, is the so-called Peng-Robinson.

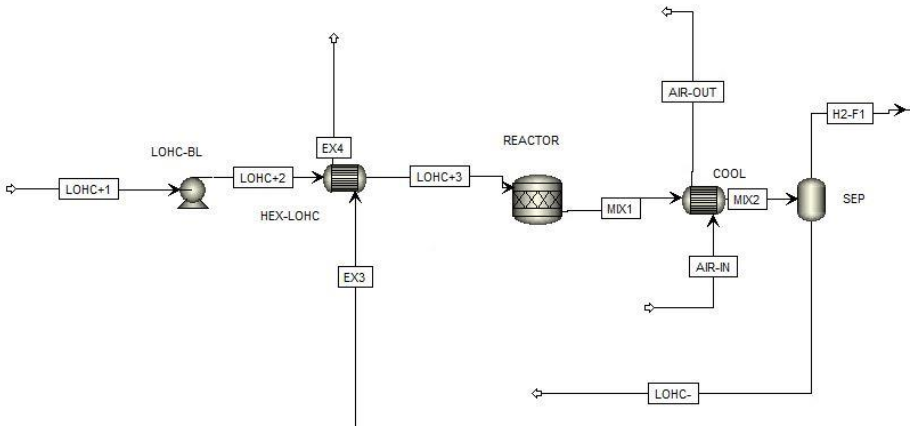

Figure 18 Hydrogen release unit

The perhydro-dibenzyltoluene (LOHC+1) is pumped into a horizontal tube reactor. Before entering the reactor, the LOHC is pre-heated using a plate heat exchanger (HEX-LOHC), where the heating media is the exhaust air coming from a catalytic burner. Concerning the pressure drop in the heat exchangers, it has been calculated automatically by Aspen Plus. The feed is introduced into the reactor, where the desorption happens. The reactor in Aspen Plus is modeled through the block "RStoic", since it allows to write the chemical reaction, for the release of hydrogen, and the degree of dehydrogenation. Then, the products, which are perhydro-dibenzyltoluene not reacted, dibenzyltoluene and gaseous hydrogen, are cooled down thanks to another plate heat exchanger (COOL), in which the cooling media is air taken from the external environment. After the cooling, the mixture goes to a flash separator (SEP) where the bottom product is H0-DBT and the top product is the gaseous hydrogen which will be used as fuel in the SOFC.

5.2. SOLID OXIDE FUEL CELL SYSTEM CONFIGURATION

In Aspen Plus does not exist a block able to simulate the behavior of a fuel cell. Therefore, as will be explained more deeply in the next chapter, this leads to separating the cathode from the anode. The anode will be simulated using a Gibbs reactor, while the cathode will be represented by a separator.

5.2.1. SOFC SYSTEM

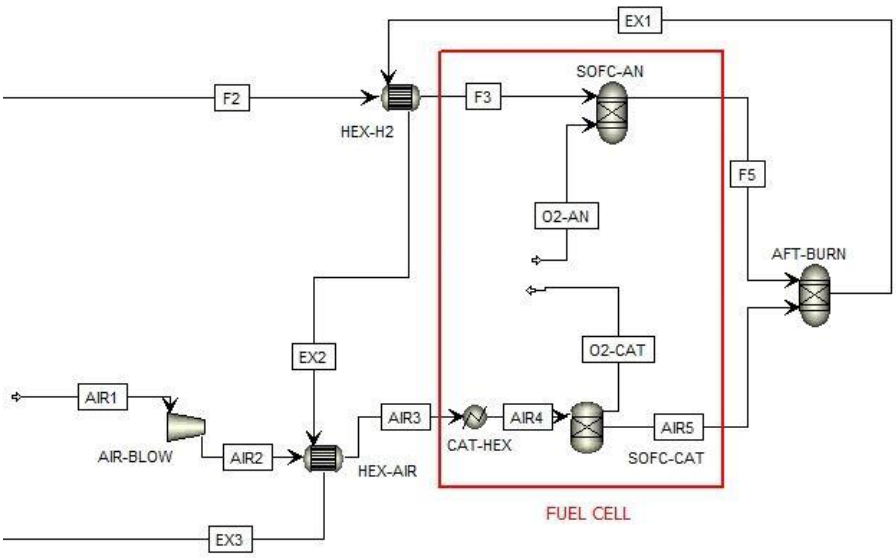

Figure 19 SOFC system

The hydrogen (F2) is coming from the hydrogen release unit. It is not compressed, since the reactor and flash separator work already in pressure. Before entering the anode, the hydrogen is preheated by a plate heat exchanger (HEX-2), in which the heating media is the exhaust air coming from the catalytic burner (AFT-BURN). Once it is preheated, the stream enters the anode. To model the anode, it has been replaced by a Gibbs reactor (SOFC-AN) to simulate the oxidation reaction. Thus, the hydrogen stream (F2) will come in contact with the oxygen (O2-AN),

producing electrical power. On the cathode side, there is the introduction of air. The airflow (AIR1) is coming from the external and it will be compressed before entering the cathode. Moreover, the stream AIR2 will be preheated always using a plate heat exchanger (HEX-AIR), where the heating media is the same air that has already preheated the hydrogen. After the preheating, the airflow enters the cathode. As can be seen in Figure 19, there is another heat exchanger (CAT-HEX). It is not a real component, because it is used to simulate the heating of the air, inside the cathode, due to the exothermic heat produced by the fuel cell. The cathode, in this case, is represented by a separator (SOFC-CAT) to simulate the reaction of recombination. So, the oxygen released (O2-CAT) will be sent to the anode.

So far, hydrogen and oxygen atoms are taken into account, but in reality, the production of power happens according to the half-reactions explained in chapter 4.2, so considering ions and electrons. The reason why, in Aspen Plus, hydrogen and oxygen atoms are considered, is that the software is not able to work with ions or electrons, but it is only able to recognize atoms or molecules.

Finally, the product streams of the fuel cell, are burned inside a catalytic burner (AFT-BURN) to obtain additional heat useful for the preheating of the hydrogen and airflow at the inlet of the fuel cell, and of the LOHC stream (LOHC+2) at the inlet of the reactor. Without the catalytic burner, the heat from the gas leaving the fuel cell alone would not be able to preheat all streams requiring heat.

5.2.2. SOFC THERMAL BALANCE

Simultaneously to the production of electrical energy, there is also a generation of heat due to two different contributions: heat of reaction and heat of transport phenomenon.

When a fuel cell produces electrical power, the heat of reaction is exothermic:

$$\phi_{REACT} = -\frac{T \cdot \Delta\bar{s}_{REACT}}{zF} \cdot I \qquad (12)$$

where:

- T is the temperature of the cell [K];
- $\Delta\bar{s}_{REACT}$ is the change in entropy of the reaction [J/mol·K];
- z is the charge number[11];
- F is the Faraday constant [s·A/mol];
- I is the cell current [A].

Instead, the heat from the irreversibility of transport processes is always exothermic. It can be generalized to the overpotentials as:

$$\phi_{IRR} = I \cdot \sum_{k=1}^{3} \eta_k \qquad (13)$$

where:

- $\eta_1$is the activation overvoltage[12];
- $\eta_2$is the ohmic overvoltage[13];
- $\eta_3$is the diffusion overvoltage[14].

Adding the two contributions, the heat produced by the cell is:

$$\phi_c = \phi_{REACT} + \phi_{IRR} = \left(-\frac{\Delta\bar{h}_{REACT}}{zF} - V_c\right) \cdot n_c \cdot I \qquad (14)$$

where:

- n_c is the number of cells;
- $\Delta\bar{h}_{REACT}$ is the enthalpy variation of the reaction [J/mol];
- V_c is the voltage of the cell [V].

[11] Charge number: number of electrons delivered or recombined of the chemical species under investigation.
[12] Activation overvoltage: drop of voltage due to the charge transfer.
[13] Ohmic overvoltage: drop of voltage due to charge migration.
[14] Diffusion overvoltage: drop of voltage due to mass transport.

Eq (14) can be also written as:

$$\phi_c = \Delta H_{REACT} - W_{el} \quad (15)$$

Since the fuel cell also produces heat, it has to be provided a specific amount of air, to cool down the stack while maintaining it at its working temperature. In this thesis, the working temperature of the SOFC is T = 850 °C.

To evaluate the mass flow rate of air needed, the following formula is used:

$$\dot{m}_{AIR} = \frac{\phi_{AIR}}{C_{p,AIR} \cdot (T_{out,air} - T_{in,air})} \quad (16)$$

where:

- $\phi_{AIR} = \phi_c$ [W];
- $C_{p,AIR}$ is the specific at constant pressure of the air [J/mol·K];
- $T_{out,air}$ is the temperature of the air at the outlet of the SOFC [°C];
- $T_{in,air}$ is the temperature of the air at the inlet of the SOFC [°C].

The calculation of the needed mass flow rate of air will be implemented in Aspen through the design specification named DS-AIR, but it will be explained in a dedicated chapter.

5.2.3. CALCULATOR BLOCKS

In Aspen Plus, it is possible to write equations in order to evaluate parameters that the software is not able to do internally. To do so, it has to be used the tool “calculator blocks” under the category “flowsheeting options”. The equations to be used in the calculator block must be written in Fortran in the section "Calculate”. Before writing the equations, it is important to define the variables that will be used in the equations, under the section “Define”.

To do so, the stages to follow are:

1. definition of the variable: give a name to the variable. It is important to give the same name to the variable, both in the sections “Define” and “Calculate”, otherwise the calculator will not work;
2. choice of the category: the equation has to be linked to a category, for example to a stream, block, reaction or others. In case the variable that is calculated is not related to any component or stream inside the flowsheet, the variable is categorized as “model utility”;
3. definition of the reference: according to the category chosen, the variable is linked for example to a specific stream or block of the model;
4. define the information flow: if a variable is used to take the information from the flowsheet, it will be marked as an “import” variable. Instead, if the value of the variable will overwrite the value of the component inside the flowsheet or it will be used to calculate a new parameter, the variable will be marked as an “export” variable.

It has to be specified, that only the variables related to components inside the flowsheet or the ones that are important to be exported, are defined in the section “define” of Aspen. Instead, the variables that will be used within the equations, for example the faraday constant or the charge number of the fuel, will be defined directly in the section “calculate”.

The reason why the calculator blocks tool is used, is to evaluate the electrical current flowing within the SOFC, the electrical power produced by the stack and the airflow needed to avoid the overheating of the stack.

5.2.3.1. C-INPUT

C-INPUT is the calculator block used to calculate the electrical current flowing in the stack (C_{tot}), the number of cells (n_c) that compose the stack and the stoichiometric quantity of oxygen ($\dot{n}_{OXY}$).

The electrical current will be evaluated as:

$$C_{TOT} = N_{FUEL} \cdot z_{H2} \cdot F \cdot FU \quad (17)$$

where:

- N_{FUEL} is the molar flow of hydrogen at the inlet of the stack. Its value is imported from the Aspen flowsheet [mol/s];
- z_{H2} is the charge number of the hydrogen, that is equal to 2;
- F is the Faraday constant [s·A/mol];
- FU is the fuel utilization of the SOFC.

Once calculated the electrical current is possible to find the number of cells as follow:

$$n_C = \frac{C_{TOT}}{(i \cdot A)} \quad (18)$$

where:

- i is the current density of the cell [A/cm^2];
- A is the active cell area [cm^2].

Finally, the molar flow of stoichiometric oxygen is calculated:

$$\dot{n}_{OXY} = \frac{C_{TOT}}{z_{O2} \cdot F} \quad (19)$$

where z_{O2} is the charge number of oxygen.

5.2.3.2. C-OXY

Once the amount of stoichiometric oxygen has been calculated in C-INPUT, it is exported into the O2-AN stream. Obviously, the same amount of oxygen (O2-CAT) must be extracted by the air entering the separator (SOFC-CAT). To do so, the calculator block “C-OXY” is used.

In particular, to make the two streams coincide the following similarity is written in the “calculate” section:

$$O2\text{-}CAT = O2\text{-}AN \quad (20)$$

5.2.3.3. C-AIR

In this calculator block, the electrical power produced by the stack and the heat that has to be removed by the mass flow rate of the air, as explained in chapter 5.2.2, are calculated.

To calculate the electrical power, firstly the voltage of the single cell has to be defined. To define it, the following formula is used:

$$V_C = OCV - ASR \cdot i \quad (21)$$

where:

- OCV is the open circuit voltage [V];
- ASR is the area specific resistance [$\Omega \cdot cm^2$].

Once the single voltage single cell is evaluated, the electrical power produced by the stack is:

$$W_{el} = n_c \cdot V_c \cdot i \cdot A$$

Then the amount of heat produced by the stack is calculated accordingly equation (15).

5.2.4. DESIGN SPECIFICATION

Design specification is another tool of Aspen Plus, always under the “flowsheeting option” section. Thanks to this tool is possible to define specific working conditions related to an equation, stream, blocks or other entities inside the model.

5.2.4.1. DS-AIR

In this section the mass flow rate of air needed to remove the heat in excess is evaluated, avoiding the overheating of the fuel cell. Initially, the heat removed by the air flow is not correct, because at the beginning it is initialized with a random value. Once the heat that has to be removed is calculated in the C-AIR block, by solving the thermal balance, through the design specification the air flow is varied to find the correct amount of air flow.

To evaluate the air flow needed, the following formula is used:

$$\dot{n}_{AIR_{real}} = \lambda \cdot \dot{n}_{AIR_{stoich}}$$

where λ is the air excess ratio.

6. ALL-ELECTRIC CASE STUDY

Once the two subsystems, the release of hydrogen and the SOFC stack, are configurated, they are joined to evaluate the technical feasibility of the entire LOHC and SOFC system.

The entire system is illustrated in Figure 20.

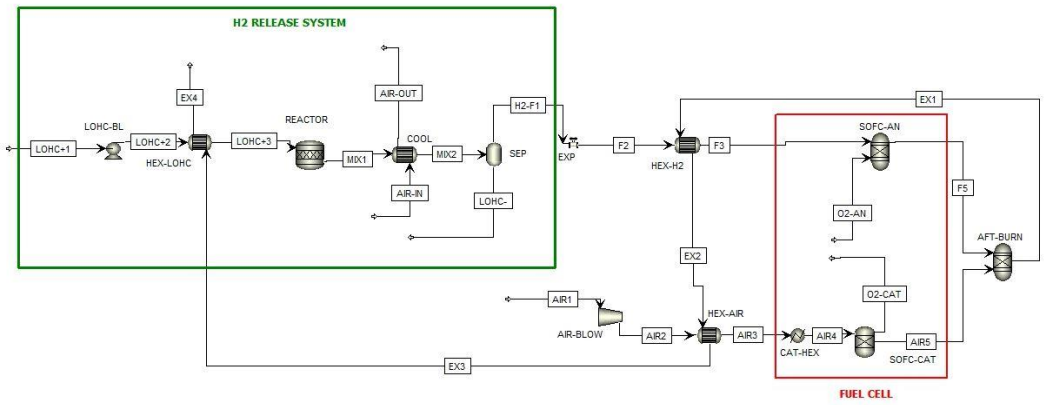

Figure 20 LOHC storage and SOFC system

As can be seen in Figure 20, the joining element is an expansion valve (EXP). In this way, also a sensitivity analysis varying the pressure of the fluids, will be performed.

6.1. SCENARIO AND WORKING CONDITIONS

Before designing each component of the system and evaluating their weight, the working condition of the all-electric case is studied.

In particular, in this thesis the aircraft studied is the ATR-72 600 whose working conditions are:

	Power [SHP]	Power [kW]	Time [min]
Take-off power	2475	1846	10
Max climb	2192	1635	17.5
Max cruise	2132	1591	120

Table 7 Power required by the ATR-72 600

It has to specify that the different power listed in Table 7, are related to a single engine. Thus, to obtain the maximum power demanded by the aircraft, the values have to be doubled. Anyway, the SOFC stack must be able to provide the maximum power requested, so it will be designed considering only the take-off power which is the largest. In this way the stack must be able to provide 3.7 MW.

To obtain such power, the following amount of hydrogen and perhydro-dibenzyltoluene are needed:

LOHC stored	8378	kg
H2 stored	498.66	kg
LOHC flow rate	0.94	kg/s
H2 flow rate	0.0563	kg/s

Table 8 Amount of H18-DBT and H_2 needed to produce 3.7 MW

The procedure to find these results is explained in chapter 6.2.1.

In the 8378 kg of perhydro-dibenzyltoluene are already taken into account the 498.66 kg of hydrogen. The SOFC stack is characterized by a fuel utilization equal to 0.7.

6.2. WEIGHT EVALUATION

In this chapter, each component will be designed in order to evaluate their weight. The weight of some components such as the tanks, the reactor and the separator will be designed more deeply than the SOFC stack, pump and compressor, since for the latter components the power density can be used.

6.2.1. H18-DBT AND H0-DBT TANK

As can be seen in Figure 3, LOHCs can be hydrogenated and dehydrogenated many times without significantly compromising the storage capacity. For this reason, once the H18-DBT is dehydrogenated, the resulting H0-DBT cannot be wasted, since it can be hydrogenated again. Therefore, two different storage tanks for H18-DBT and H0-DBT have to be provided. To design the tank size and weight, firstly the volume of the hydrogenated/dehydrogenated liquid has to be found. To do so, the weight of the hydrogen and consequently the one of the perhydro-dibenzyltoluene are considered. Considering a flight of 147.5 min, the amount of hydrogen needed by the airplane is 498.66 kg, as included in Table 8. Then, it is possible to evaluate the amount of LOHC as:

$$m_{H18-DBT} = \frac{m_{H_2}}{wt\%H_2 \cdot DoD} = 8378\ kg \qquad (22)$$

where:

- $wt\%H_2$ is the gravimetric index of dibenzyltoluene, that is equal to 6.2%;
- DoD is equal to 96%. It is taken into account since, it means that the only 96% of hydrogen is desorbed.

By knowing the mass of H18-DBT, it is possible to evaluate the volume of the tank just dividing for its density. Once the volume is known, it is possible to design the dimensions of the tank.

Particularly, the shape of the tank is the following:

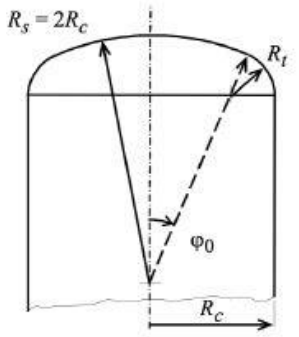

Figure 21 Shape of the LOHC tank

Therefore, the tank has a cylinder body, with two portions of sphere as endplates. The conjunction between the endplates and the cylinder body is done through a toroid. In Figure 21, there are: R_c which is the radius of the cylinder, R_s that is the radius of the sphere, R_t which is the radius of the toroid and φ_0 is the angle used to find the position of the transition between the sphere and the toroid.

This shape is chosen as a function of the tank wall material, that is aluminum. For isotropic materials, to achieve a continuitity in the strain between the junctions, a shape like the one in Figure 21 needs:

$$R_s = 2 \cdot R_c \tag{23}$$

and

$$R_t = \frac{R_s}{10} \tag{24}$$

To find the correct point, where there should be the transition between the sphere and the toroid, to guarantee a continuity in the strain between the junction, the following formula is used:

$$sin\varphi_0 = \frac{Q\prime \cdot C_\varphi}{O \cdot C_\varphi} = \frac{R_C - R_t}{R_S - R_t} \tag{25}$$

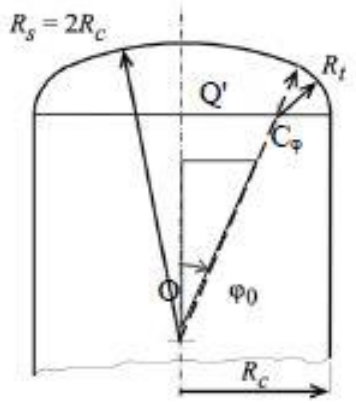

Figure 22 Shape of the tank for the determination of φ_0

Once defined the reason why that shape is chosen, knowing the volume of LOHC and fixing the radius of the cylinder, the dimensions of the tank can be calculated consequently. The data related to the tank are listed in Table 9.

Input	**V_{LOHC} [m^3]**	**R_c [m]**		
	8.06	0.5		
Output	**R_s [m]**	**R_t [m]**	**l [m]**	**φ_0 [deg]**
	1	0.1	9.77	26.4

Table 9 H18-DBT dimensions

where "l" is the length of the cylinder.

After the definition of the tank geometry, the thickness of the tank is evaluated through the membrane theory.

Firstly, the maximum internal pressure of the tank has to be calculated in order to evaluate the thickness of the tank. To do so, the following procedure is used [35]:

$$\Delta p = p_{op} - p_{amb} \qquad (26)$$

where: p_{op} is the operating pressure inside the tank in normal conditions and p_{amb} is the external pressure at cruise height.

Then, the limit design pressure is calculated as:

$$p_{des} = 1.1 \cdot \Delta p \quad (27)$$

The differential pressure is multiplied by 1.1 to take into account the inertia. Finally, the maximum allowable pressure is:

$$p_{burst} = 2 \cdot p_{des} \quad (28)$$

At the burst pressure the catastrophic failure of the tank is not permitted.

Once the internal pressure is evaluated, it is possible to proceed in the calculation of the tank wall thickness. Thus, the membrane stresses are calculated. For the cylinder the membrane stresses are:

$$n_{\varphi c} = \frac{p_{burst} \cdot R_c}{2} \quad (29)$$

$$n_{\theta c} = p_{burst} \cdot R_c \quad (30)$$

where $n_{\varphi c}$ and $n_{\theta c}$ are the meridian and circumferential membrane stresses, respectively. Then the membrane stresses of the sphere are calculated as:

$$n_{\varphi s} = \frac{p_{burst} \cdot R_s}{2} \quad (31)$$

$$n_{\theta s} = \frac{p_{burst} \cdot R_s}{2} \quad (32)$$

where $n_{\varphi s}$ and $n_{\theta s}$ are the meridian and circumferential membrane stresses, respectively.

Concerning the toroid, it is assumed as a a cylinder since its contribution is quite small.

Then it is possible to evaluate the stresses according to:

$$\sigma_{\varphi} = \frac{n_{\varphi}}{t} \quad (33)$$

$$\sigma_{\theta} = \frac{n_{\theta}}{t} \quad (34)$$

where “t” is our unknown. Eq. (33) and (34) are valid for the cylinder, sphere and toroid. To evaluate the thickness and consequently the stresses, it has to be considered the ideal stress. Indeed, knowing the yield stress (Rp_{02}) of the aluminum and choosing a safety factor (SF), the ideal stress (σ_{id}) is calculated as:

$$\sigma_{id} = \frac{Rp_{02}}{SF} \quad (35)$$

The ideal stress can be also written as:

$$\sigma_{id} = \sigma_1 - \sigma_3 \quad (36)$$

where σ_3 is the minimum stress and σ_1 is the maximum stress. Particularly, σ_3 is always the radial stress (σ_r) calculated as:

$$\sigma_r = -p_{burst} \quad (37)$$

while σ_3 could be σ_φ or σ_θ depending on the geometry considered.

For the cylinder:

$$n_{\theta c} = 2 \cdot n_{\varphi c} \quad (38)$$

Thus:

$$\sigma_{\theta c} = 2 \cdot \sigma_{\varphi c} \quad (39)$$

This means that σ_1 is equal to $\sigma_{\theta c}$.

In the case of the sphere:

$$n_{\theta s} = n_{\varphi s} \quad (40)$$

This means that σ_1 could be equal to $\sigma_{\theta s}$ or $\sigma_{\varphi s}$.

Once the minimum and maximum stresses are found, they are rewritten as a function of the membrane stresses, according to eq (33) and (34). Then, the resultant equations are written as a function of the burst pressure according to eq (29) and (30) for the cylinder, and eq (31) and (32) for the sphere.

Thus, in case of the cylinder, eq (36) can be written as:

$$\sigma_{id} = \sigma_r - \sigma_{\theta c} = -p_{burst} - \frac{p_{burst} \cdot R_c}{t} \quad (41)$$

At the same time, in case of the sphere, eq (36) is written as:

$$\sigma_{id} = \sigma_r - \sigma_{\theta c} = -p_{burst} - \frac{p_{burst} \cdot R_s}{t} \quad (42)$$

In both eq (41) and (42), the only unknown is the thickness (t) that can be finally evaluated. For the toroid is assumed the larger thickness between the one of the spheres and the cylinder. Knowing the thickness, it is calculated the volume occupied by the aluminum, which is used to evaluate the weight of each section:

$$W_c = V_c \cdot \rho_{Al} \quad (43)$$

$$W_s = V_s \cdot \rho_{Al} \quad (44)$$

$$W_t = V_t \cdot \rho_{Al} \quad (45)$$

where:

- W_c, W_s and W_t are the tank wall weights of the cylinder, sphere and toroid sections;
- V_c, V_s and V_t are the volumes occupied by the cylinder, sphere and toroid section with thickness "t";
- ρ_{Al} is the density of the aluminum.

Finally, the total weight of the tank is calculated as:

$$W_{tank\_wall} = W_c + 2\,W_s + 2\,W_t \quad (46)$$

The weight of the sphere and toroid is multiplied by two, since there are two semisphere endplates and two toroidal junctions. Then, through the same procedure used fo the H18-DBT storage tank, the weight of the H0-DBT storage tank can be calculated. So, knowing the volume of H0-DBT and the one of the H18-DBT, and fixing the raius of the cylinder, the weight of the dehydrogenated LOHC is computed. The H18-DBT unreacted, since the DoD is 96%, will be

equal to 4%, thus it has to be separated by the hydrogen and stored together with the H0-DBT. The input data for the evaluation of the weight are:

Input	Rp_{02} [Mpa]	SF	p_{burst} [bar]	ρ_{Al} [kg/m3]
	193	2	1.37	2680

Table 10 Input data for the weight calculation of H18-DBT/H0-DBT in the all-electric case

For the all-electric case, the volume and weight results of the tank are listed in Table 11:

Tank	Volume [m^3]	Weight [kg]
H18-DBT	8.08	65.69
H0-DBT	8.73	70.62

Table 11 Weight and volume contribution of the LOHC tanks in the all-electric case

The reason why the volume of H0-DBT tank is larger is related to the lower density of the latter with respect to H18-DBT. Consequently, the weight of H0-DBT tank will be higher than the one of H18-DBT because of the more aluminum.

6.2.2. HORIZONTAL TUBE REACTOR

To desorb the hydrogen from perhydro-dibenzyltoluene a horizontal tube reactor, filled with a fixed bed of catalyst, is used. Moreover, it is only half-filled with liquid [23]. A representation of the reactor is presented in the following picture:

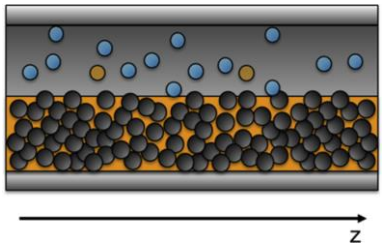

Figure 23 Horizontal tube reactor scheme [23]

In Figure 23, the block dots represent the catalyst bed, the blu dots illustrate the the hydrogen desorbed and the orange color is used to represent the flowing of perhydro-dibenzyltoluene.

To evaluate the weight of the reactor, its volume has to be defined. Once the volume of the reactor will be computed, the volume of catalyst will be calculated. By knowing the two volumes and the materials' densities, the weight of the entire reactor (tank wall and catalyst bed) will be then evaluated.

The main parameters influencing the reactor volume are the volumetric flow of LOHC, the Liquid Hourly Space Velocity (LHSV), the residence time, the temperature of dehydrogenation and the DoD.

To find the value of LHSV, the map represented in Figure 24 is used.

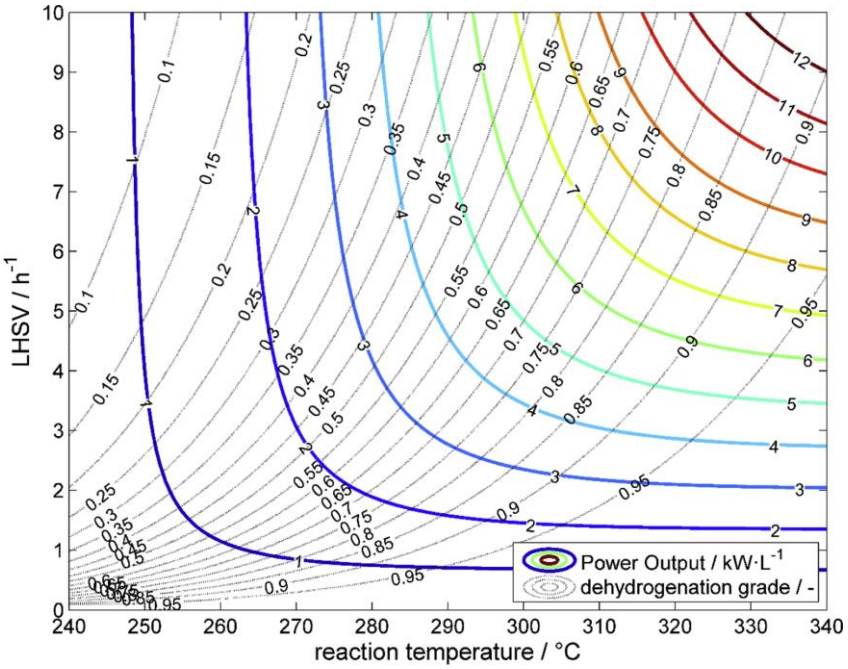

Figure 24 Map of the dehydrogenation grade as a function of the LHSV [23]

Thus, considering a reaction temperature and a DoD, a value of LHSV is obtained. The the reactor volume is calculated according to:

$$V_{react} = \frac{\dot{V}_{LOHC}}{\epsilon \cdot F_{RV}} \qquad (47)$$

where:

- $\dot{V}_{LOHC}$ is the volumetric flow rate of perhydro-dibenzyltoluene entering the reactor;
- ϵ is the porosity of the catalyst bed;
- F_{RV} is the fraction of active reactor volume.

Once the volume of the reactor is known, its weight is evaluated by following the procedure used for the evaluation of the thickness of the H18-DBT or H0-DBT tank. Therefore, knowing the volume, the thickness of the tank is found and finally the weight is calculated.

Then, the catalyst volume is calculated as:

$$V_{cat} = \frac{\dot{V}_{LOHC}}{LHSV} \quad (48)$$

Thanks to its density, the weight of the catalyst (Pt/Al_2O_3) is found.

Finally, the weight of the reactor is calculated as:

$$W_{react} = W_{cat} + W_{wall\_react} \quad (49)$$

where W_{cat} is the weight of the catalyst and W_{wall_react} is the weight of the wall of the reactor, made of stainless steel.

The required inputs are summarized in Table 12, while the results in Table 13:

T [K]	DoD	V_{LOHC} [m^3/h]	ε	F_{RV}
320	0.96	4.49	0.4	0.8
ρ_{cat} [kg/m^3]	ρ_{ss} [kg/m^3]	Rp_{02} [Mpa]	SF	p_{burst} [bar]
970	7850	280	2	5

Table 12 Input for reactor weight evaluation in the all-electric case

V_{react} [m3]	V_{cat} [m3]	W_{wall_react} [kg]	W_{cat} [kg]	W_{react} [kg]
5.40	1.73	318.87	1676.62	1995.49

Table 13 Weight of the reactor for the all-electric case

It has to be specified that the reactor working conditions are: temperature equal to 320 °C and pressure equal to 2 bar. Thus, the burst pressure is just used for the structural design of the reactor.

6.2.3. FLASH SEPARATOR

To separate the gaseous hydrogen from the dibenzyltoluene, a flash separator working at a temperature of 60 °C and a pressure of 2 bar is used. In particular, a horizontal separator is used. It is preferred a horizontal separator with respect to a vertical one, because the height of the separator is such that it cannot fit into the fuselage. Moreover, horizontal separators allow to have a smaller diameter than vertical separators for the same gas capacity.

To design the flash separator and to evaluate its weight, firstly the gas and then the liquid capacity has to be calculated [36]. To evaluate the gas capacity, the superficial gas velocity (v) is found as:

$$v = K\left[\frac{\rho_L - \rho_g}{\rho_g}\right]^{1/2} \quad (50)$$

where:

- K is an empirical factor whose value is calculated in reference [36];
- ρ_L is the density of the LOHC;
- ρ_g is the density of the gaseous hydrogen.

Then the cross-sectional area of the separator available for the vapor flow (A) is calculated as:

$$A = \frac{q}{v} \quad (51)$$

where “q” is the hydrogen flow rate entering the separator.

After the evaluation of the gas capacity, the liquid settling volume is computed as follows:

$$V = \frac{W \cdot t}{1440} \quad (52)$$

where “W” is the liquid capacity and “t” is the retention time.

It is calculated the liquid settling volume since the manufacturers give the dimensions of the separator as a function of the total settling volume. Indeed, once the settling volume is known, according to TABLE 3B in the reference [36], the size of the separator is known. Finally, thanks to the size of the separator, the weight is found through the ASME sizing charts [37].

The input needed for the evaluation of the gas capacity are:

ρ_{H2} [kg/m3]	ρ_{LOHC} [kg/m3]	K	q_{H2} [m3/s]
0.162	19.910	0.565	0.347

Table 14 Input for evaluation of separator gas capacity in the all-electric case

It has to be specified that at the outlet of the reactor, there will be two liquids which are H0-DBT and the unreacted H18-DBT, whose amount is very low in comparison with the one of H0-DBT. Anyway, a mean density as a function of the flow rate has been calculated and it is the one ($\boldsymbol{\rho_{LOHC}}$) in Table 14.

The results obtained are a superifical gas velocity $v = 6.23\, m/s$ and an area available for the vapor flow $A = 0.009\, m^2$.

At the same time, the input for the evaluation of the liquid settling volume (V) are the liquid capacity W = 23967.8 bbl/day and a retention time t = 1 min. In this way it is obtained $V = 16.64\, bbl$. The liquid capacity is calculated considering both H18-DBT and H0-DBT, while the retention time is considered equal to 1 minute according to reference [36]. Always thanks to reference [36], by knowing the settling volume, the dimensions of the separator can be obtained and they

resulted to be 48” x 15’. Once the dimensions are defined, through ASME sizing charts [37], the weight of the separator is found, and it is equal to 1156.68 kg.

6.2.4. LOHC PUMP

To evaluate the pump weight, it is considered a commercial pump produced by Wilo[15]. In particular, it is chosen the product HiMulti which is able to pressurize liquids up to 8 bar. Thus, checking on the catalog, the pump HiMulti 3-24/1/5/230/S1 is chosen, and it is characterized by a nominal power P_n = 0.4 kW for a weight of about 10.3 kg. Thank to this data, the specific power is calculated and it is equal to 38.9 W/kg. Once the specific power is known it is possible to evaluate the weight of the pump needed for the all-electric case.

The pump in the all-electric case must increase the pressure from 1 to 2 bar of an H18-DBT flow rate equal to 0.94 kg/s. Therefore, the power required by the pump is 113.52 W, which divided by the specific power calculated above leads to a pump weight equal to 2.92 kg.

6.2.5. SOFC STACK

To design the SOFC stack, are taken reference values from the literature. First of all, the parameter characterizing the cell voltage, calcuted using eq (21), are: OCV = 0.98 V, ASR = 0.5 $\Omega \cdot cm^2$ and i = 583 mA/cm^2 [38]. The cell voltage is calculated in this way, in order to represent a behavior more similar to the reality. Then, to evaluate the weight it is used a reference value of power density, always from the literature, which is 467 W/kg [39]. In this way, dividing the stack power, whose value is 3.7 MW, by the specific power, the weight of the stack is found and it is equal to 7922.9 kg.

[15] Wilo is a european manufacturer of pumps and pumping system located in Dortmund, Germany.

6.2.6. COMPRESSOR AND HEAT EXCHANGERS

The compressor for the all-electric case has to deal with an airflow of 6.45 kg/s. Particularly, it has to increase the pressure of the mass flow rate from 1 bar to 1.6 bar. The value of 1.6 bar is chosen in order to take into account the pressure drop through the heat exchangers and thus avoid a subatmospheric pressure after passing through all the heat exchangers. In order to pressurize that amount of air up to 1.6 bar, the power required by the compressor is 464.6 kW. Once the power demanded is known, a reference value of specific power taken from the literature will be used to calculate the compressor weight. Thus, by choosing the value of specific power, which is 1.88 kW/kg [40], and dividing the power required for it, the weight of the compressor is 247.77 kg.

Concerning the weight evaluation of the heat exchangers, the procedure is completely done automatically by Aspen. Indeed, through the temperatures and mass flow rates of the streams, and selecting an estimated pressure drop and a type of heat exchanger the software returns the number of heat exchangers needed and their weight. The type chosen is a plate heat exchanger produced by Tranter while the estimated pressure drop is 0.14 bar. Concerning the air used at the inlet of the cathode and the one used to cool down the products exiting the reactor, it is chosen to be under ambient conditions at ground level and not at the cruising height. This choice is made since the compression ratio is lower at ground level than the one at cruising height. Therefore, the air temperature exiting the compressor would be higher than the one in the case at ground level, leading to a positive effect from the heat exchange point of view. Indeed, there would be a lower gradient of temperature to satisfy, leading to a smaller heat exchanger. In this thesis, is chosen to study the heat management of the system at ground level, because it represents the worst scenario.

The inputs needed for the evaluation of the weight are listed in Table 15:

	LOHC+2	LOHC+3	MIX1	MIX2	AIR-IN
Mass flow rate [kg/s]	0.94	0.94	0.94	0.94	6
Temperature [°C]	25	300	320	60	25
	F2	**F3**	**AIR2**	**AIR3**	**EX1**
Mass flow rate [kg/s]	0.056	0.056	6.45	6.45	6.51
Temperature [°C]	60	800	81.9	700	1097.7

Table 15 Input needed for plate heat exchanger weight evaluation in the all-electric case

Thanks to these data, Aspen returns the weight of the heat exchanger which are:

	HEX-H_2	HEX-AIR	HEX-LOHC	COOL-LOHC
Number	2	2	1	1
Single Hex Weight [kg]	3493	2616.4	4343	4343
Tot Weight [kg]	6986	5232.8	4343	4343
Single Volume [m^3]	3.85	2.89	4.80	4.80
Tot Volume [m^3]	7.71	5.77	4.80	4.80

Table 16 Weight and volume of plate heat exchangers for the all-electric case

As can be seen in Table 16, in order to preheat the hydrogen and the air entering the SOFC are needed two heat exchangers each.

6.3. TOTAL WEIGHT AND GRAVIMETRIC INDEX OF H_2 STORAGE

Once the weight of each component has been calculated, it is possible to determine the weight of the hydrogen storage systems and of the SOFC stack considering also the balance of plant.

The results obtained are:

	HYDROGEN SYSTEM	SOFC SYSTEM	TOTAL
Weight [kg]	20355	20389	40745
Volume [m3]	37.14	18.24	55.38

Table 17 Weight and volume of each system in the all-electric case

Finally, by knowing the total weight of the hydrogen storage system, its gravimetric index can be computed as follow:

$$wt\%\ H_2 = \frac{m_{H_2}}{W_{tot\_H2\_syst}} = 2.45\ \% \qquad (53)$$

It has to be specified that in the evaluation of the gravimetric index are considered also the reactor, the separator, the pump, the H18-DBT and H0-DBT tanks and heat exchangers necessary for heating and cooling of the LOHC.

6.4. CONSIDERATIONS

Once the weight of each component and the one of the overall system is known, it is interesting to evaluate the impact, in terms of percentage, of the components on the overall system indeed.

To do so, the pie chart represented in Figure 25.

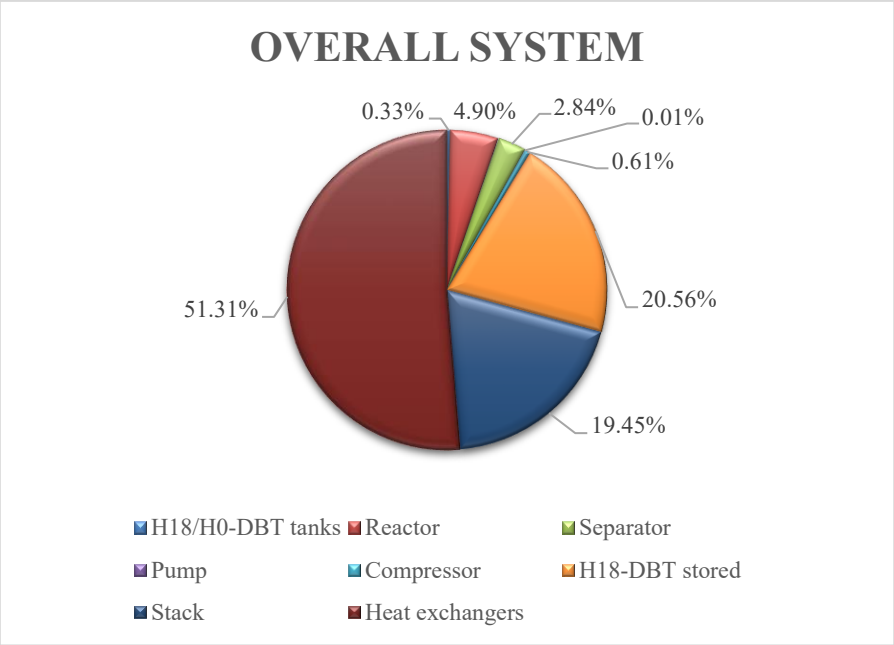

Figure 25 Weight contribution in terms of percentage of each component with respect to the entire system weight

As can be seen in Figure 25, the most impacting weight on the overall system are the H18-DBT stored, that takes into account the mass of H_2 necessary for the flight, the heat exchangers needed for pre heating the streams and the SOFC stack.

Then the feasibility of the all-electric ATR-72 600 is evaluated by comparing the weight of the entire "LOHC-SOFC system" plus the electric motors with the weight requirement of the ATR-72 600 [41].

The maximum take-off weight (MTOW) of the conventional aircraft is 22800 kg. The MTOW of the all-electric case includes the weight of the aircraft structrure and propellers, of the H_2 release system, of the SOFC system and two electric motors. The weight of the aircraft structure and propellers is found by subtracting the weight of the thermal system, thus:

$$W_{aircraft_{struc}\&prop} = MTOW_{conv} - W_{thermal_{system}} = 18369.9 \quad (54)$$

where $W_{thermal_{system}}$ is the weight of the termal system which includes the fuel, the kerosene system and the two thermal engine and it is equal to 4430.07 kg.

The weight of the H_2 release and SOFC system are included in Table 17. Then to evaluate the weight of the two electric motors, a power density of 5.2 kW/kg [42] is considered. Thus, considering the electrical power, the overall weight of the electric motors is 712 kg. Finally considering the weight of the aircraft structure and propellers, of the H_2 release and SOFC system and of the electric motors, the MTOW of the all-electric case is 59826 kg.

It is more than 30000 kg higher than the maximum required. Therefore, as can be easly understood, the all-electric case, for the technologies available nowadays, is not feasible.

Moreover, the H_2 storage system is not even competitive with the thermal system. Indeed, the latter has a weight of about 4430.07 kg, while the only hydrogen storage system has a weight of 20355 kg.

The contribution of each weight to the MTOW and the comparison between the conventional and the all-electric MTOW can be seen in Figure 26.

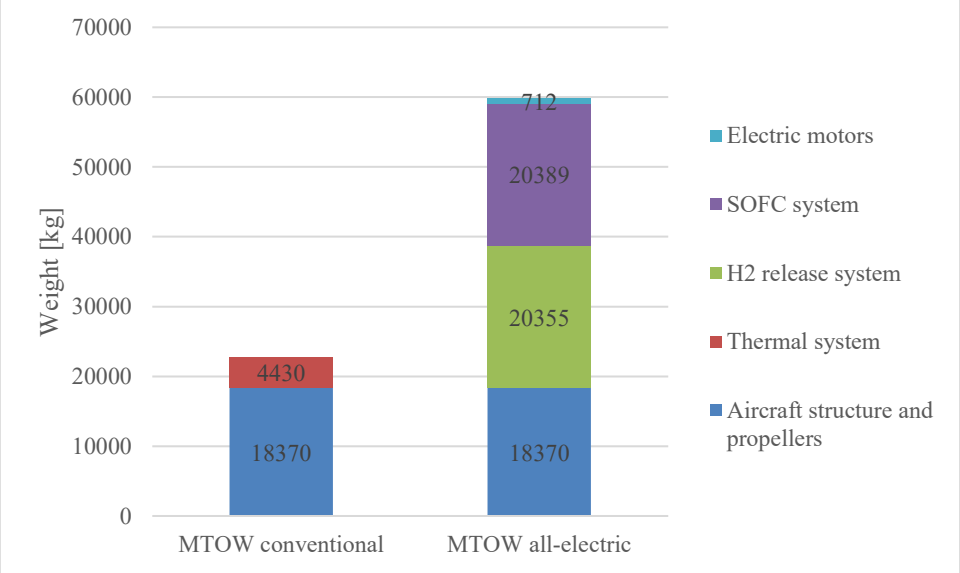

Figure 26 Comparison between the conventional and all-electric MTOW

Another interesting consideration can be done as a function of the number of passengers that should be removed to have the same MTOW as the conventional aircraft. The ATR-72 600 is able to transport 72 passengers, but to achieve the

same MTOW the number of passengers that should be removed is equal to 427, so even higher than the number of passengers that the aircraft is able to transport.

Therefore, firstly a sensitivity analysis will be done in order to evaluate if the all-electric case can be improved, reducing the weight and checking again its feasibility. If even after the improvement, the system is not feasible, the best configuration of the all-electric case will be used to study different degree of hybridization.

7. SENSITIVITY ANALYSIS

To choose which parameters need to be changed in the sensitivity analysis, the Figure 25 is considered. Being the heat exchangers and the H18-DBT stored, the most impactin weight, a sensitivity analysis on the fuel utilization of the stack will be performed to reduce the amount of hydrogen and consequently the amount of H18-DBT, that must be stored. Then a second sensitivity analysis will be performed increasing the pressure of the fluid entering the stack, to increase the turbulence of the streams, thus enhancing the heat transfer in the heat exchangers. Lastly, the pressure drops across each heat exchangers will be increased, in order to increase, also in this case, the heat transfer in the heat exchangers. Thanks to these two methods the weight of the heat exchangers, should be reduced.

7.1. FUEL UTILIZATION

In this chapter, the fuel utilization of the SOFC will be varied between 0.7 and 0.85. Values higher than 0.85 are not studied, because SOFCs able to work at these values do not exist. The reason why, the FU is varied, is to reduce the amount of hydrogen required by the SOFC to produce 3.7 MW. Indeed, as can be seen in eq (17), keeping constant the electrical current flowing within the stack (CTOT), the increase of the FU allows to reduce mass flow rate of hydrogen needed (NFUEL). Moreover, a lower amount of stored hydrogen, leads to a decrease in the amount of H18-DBT stored, whose represents the 20.56% of the overall weight.

The FU can be represented as:

$$FU = \frac{\dot{m}_{H_2\,REAL}}{\dot{m}_{H_2\,TOT}} \qquad (55)$$

where $\dot{m}_{H_2\,TOT}$ is the total amount of hydrogen flowing within the anode and $\dot{m}_{H_2\,REAL}$ is the hydrogen flow rate that effectively react to produce power.

Increasing the FU will decrease the amount of hydrogen that must be stored, but on the contrary, there will be a lower amount of unreacted hydrogen exiting the anode exhaust. Thus, a lower heat production in the catalytic burner will happen. The results related to the reduction of the mass flow rates and the masses to be stored, and the lower temperature of the catalytic burner exhaust gases are listed in Table 18.

FU	0.7	0.75	0.8	0.85
H_2 flow [kg/s]	0.056	0.053	0.049	0.046
H_2 stored [kg]	498.66	465.41	436.32	410.65
H18-DBT flow [kg/s]	0.94	0.88	0.82	0.77
H18-DBT stored [kg]	8378	7819	7331	6899
H_2 unreacted [kg/s]	0.017	0.013	0.010	0.007
Exhaust Temp [°C]	1097.7	1044	996.5	954

Table 18 Variation of the mass flow rates, stored masses and exhaust gas temperature of the catalytic burner as a function of the FU

As can be seen in Table 18, thanks to the FU increase, the weight of H18-DBT stored is decreased by 1478 kg, more or less. Simultaneously, a decrease of about 143.7 °C for the temperature of the exhaust gas exiting the catalytic burner occurs. Thus, in addition to not existing fuel cells with a FU greater than 0.85, it would not be convenient to go further since the possibility of pre-heating the system would be lost.

The evolution of the H_2 flow at the inlet and at the outlet of the anode, and the consequent reduction of stream temperature exiting the after burner, as a function of the FU, can be better displayed in Figure 27.

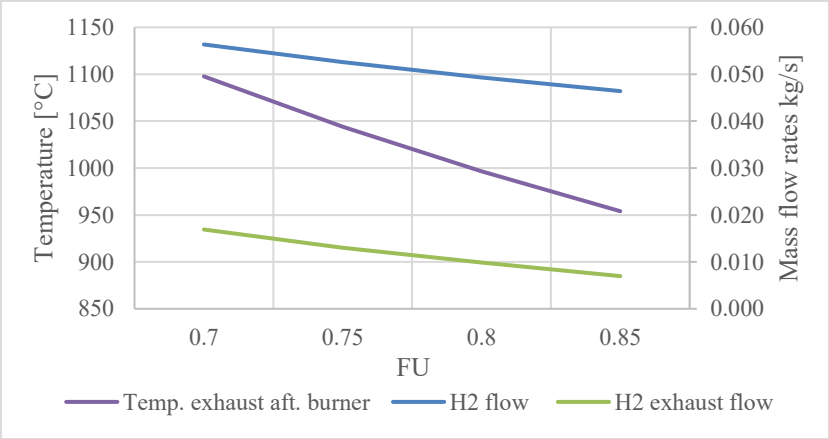

Figure 27 Evolution of the H_2 flow entering and exiting the anode, and of the gas temperature exiting the catalytic burner

The decrease in the H18-DBT and hydrogen flow rate leads to a decrease in the dimensions of the pump, the reactor and of the H18-DBT and H0-DBT tanks. Concerning the separator, unfortunately, the decrease in the mass flow rates is not enough to ensure a decrease in the size of it, reason why its weight will not vary as a function of the FU. Other consequences related to the increase of FU are related to the weight reduction of the plate heat exchangers. In this case the reduction is mainly due to the decrease of the mass flow rates flowing within the heat exchangers. The weight of each component as a function of the FU is represented in Table 19.

FU	0.7	0.75	0.8	0.85
H18-DBT tank [kg]	65.69	61.59	58.00	54.83
H0-DBT tank [kg]	70.62	66.18	62.31	58.89
Reactor [kg]	1995	1863	1748	1646
Separator [kg]	1156.7	1156.7	1156.7	1156.7
Compressor [kg]	247.8	248.4	249.0	249.4
Pump [kg]	2.92	2.72	2.55	2.40
HEX-H2 [kg]	6986	6826.6	6720.4	6614.2
HEX-AIR [kg]	5232.8	5020.4	4807.8	4595.4
HEX-LOHC [kg]	4343	4024.3	3811.8	3625.8
COOL-LOHC [kg]	4343	4024.3	3811.8	3625.8
SOFC stack [kg]	7923	7923	7923	7923

Table 19 Weight of each component as a function of the FU

The weight of the hydrogen release system, of the SOFC system and of the entire system is included in

FU	0.7	0.75	0.8	0.85
H2 RELEASE SYSTEM [kg]	20355	19019	17982	17070
SOFC SYSTEM [kg]	20389	20018	19700	19382
GLOBAL SYSTEM [kg]	40745	39037	37682	36452

Table 20 Weight of each subsystem and of the global system

To better visualize the results obtained, the following graph is used:

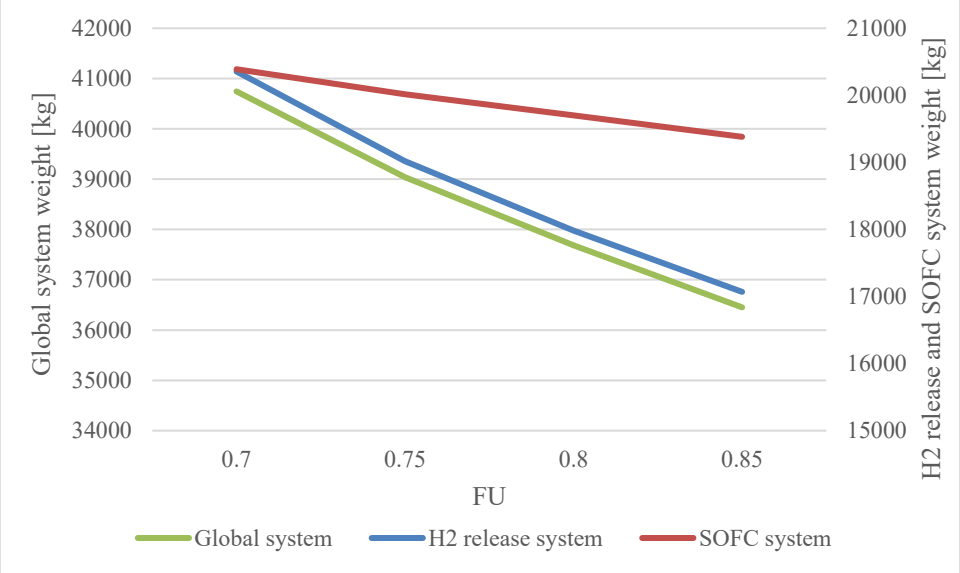

Figure 28 Evolution of the H2 release, SOFC and global system as a function of the FU

As can be seen, this sensitivity analysis has a major impact on the hydrogen release system. Indeed, the goal of this sentivity analysis is to reduce the need of hydrogen from the SOFC, reducing consequently the mass flow rate of H18-DBT flowing into the reactor and separator. Thus, decreasing their size and weight. Moreover, the reduction of hydrogen required by the stack leads to reduce the amount of H18-DBT that has to stored.

As a result of the increase in FU, there is a decrease of about 3000 kg in the H_2 release system and of about 1000 kg in the SOFC system, leading to an overall decrease in weight equal to 4000 kg.

Focusing on the most impacting components on the weight of the overall system, which are the H18-DBT stored and the plate heat exchangers, their weight reduction is represented in Table 21.

FU	0.7	0.75	0.8	0.85
H18-DBT stored [kg]	8378	7819	7331	6899
HEXs [kg]	20905	19896	19152	18461
H18-DBT stored [%]	20.56	20.03	19.45	18.93
HEXs [%]	51.31	50.97	50.83	50.65

Table 21 Weight and percentage contribution on the overall system of H18-DBT stored and heat exchangers

The voice "HEXs" takes into account the weight of all heat exchangers in the system.

As can be seen in Table 21, the increase of the FU leads to decrease the impact of the H18-DBT stored and of the heat exchangers on the overall systems of 1.63% and 0.66%, respectively. The percentage contribution of each component considering a FU=0.85 and a pressure of the fluids entering the SOFC stack of 1.6 bar is represented in Figure 29.

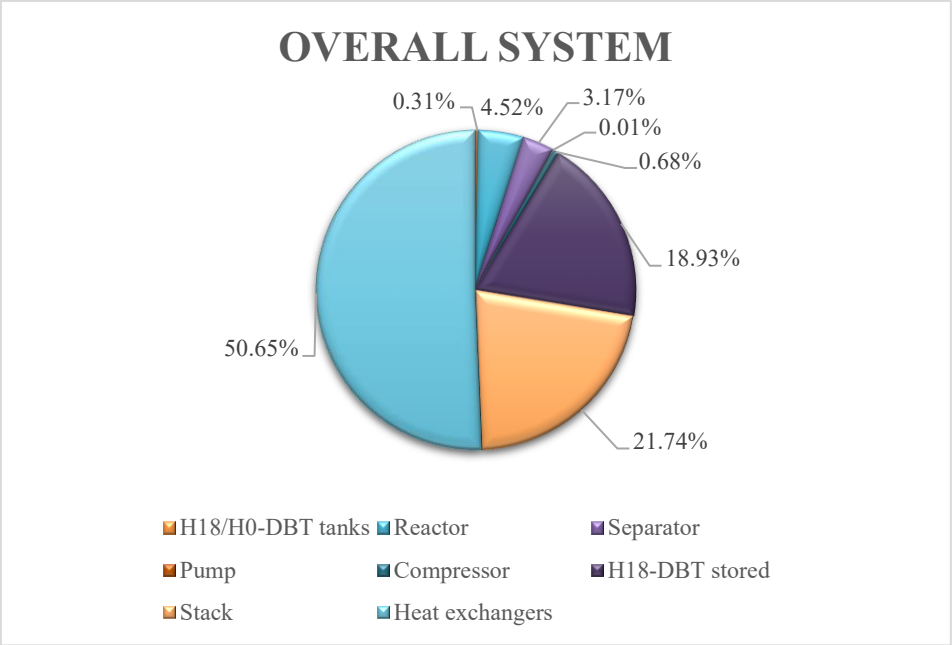

Figure 29 Percentage contribution of each component in terms of weight with a FU=0.85

The results related to the gravimetric index of the hydrogen storage system are listed in the following table:

FU	0.7	0.75	0.8	0.85
wt%H2	2.45	2.447	2.426	2.406

Table 22 Gravimetric index of H_2 storage system

As can be seen in Table 22, increasing the FU, the gravimetric index decreases. This could be explained by the fact that while the H_2 stored is reduced, the weight of the separator remains the same.

Even though with a FU = 0.85, the gravimetric index is the worst, this configuration will be chosen to be used as base case to make a further sensitivity analysis on the pressure of the fluids entering the SOFC stack. The main reason of choosing the configuration of FU = 0.85 is related to the weight saved.

7.2. FLUID PRESSURE ENTERING THE SOFC STACK

In Figure 29, the most impacting components are the heat exchangers. For this reason, in this chapter the fluids entering the SOFC will be varied between 1.6 bar, which is the best configuration of the previous chapter, to 2 bar. In this way, the turbulence of the streams should increase, leading to an improvement in the heat transfer and thus a lower heat exchanger is needed. Besides, increasing the compression ratio, the stream temperature will be higher, thus a lower amount of heat has to be provided to the airflow before entering the cathode. However, there is a drawback related to the increase in weight of the compressor.

The results obtained are listed in Table 23:

Pressure [bar]	**1.6**	**1.8**	**1.9**	**1.95**	**2**
Compressor [kg]	249.44	317.38	349.34	364.87	384.92
Hex-H_2 release system [kg]	7252	6667	6614	6508	6349
Hex-SOFC system [kg]	11210	7655	7347	7256	8697
Hex-TOT [kg]	18461	14323	13961	13764	15045

Table 23 Compressor and heat exchangers weight reduction as a function of the pressurization

where the voice "Hex-H_2 release system" includes the heat exchangers (HEX-LOHC and COOL) for heating and cooling the streams entering and exiting the reactor, while the voice "Hex-SOFC system" includes the heat exchangers (HEX-H2 and HEX-AIR) for heating the hydrogen entering the anode and the air entering the cathode.

Even in this case, to better visualize the evolution of the plate exchangers' weight as a function of the pressurization, the following graph is used:

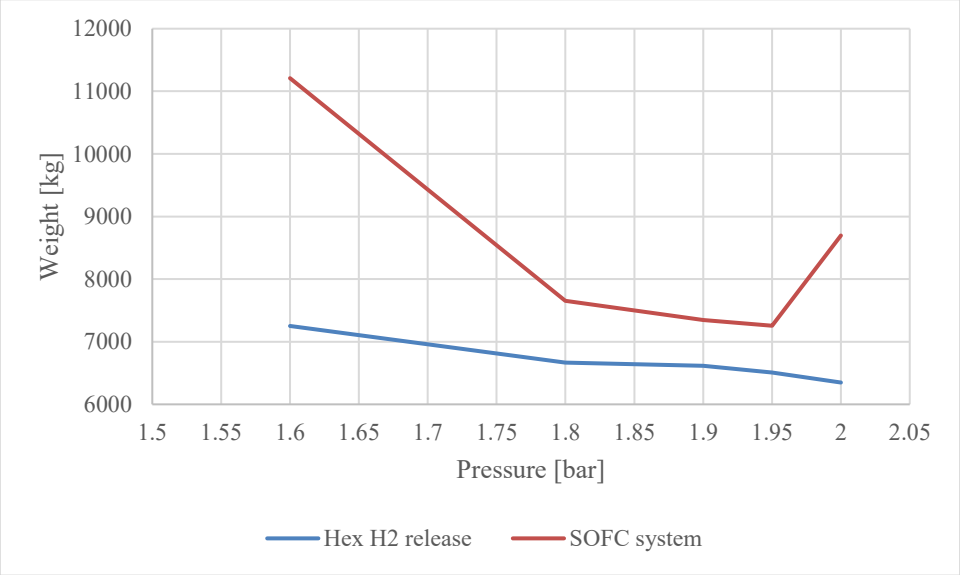

Figure 30 Heat exchangers weight reduction as a function of the pressurization

As can be seen in Figure 30, increasing the pressure leads, in most of the cases, to a decrease in weight. Looking, however, the case in which the pressure is set at 2 bar, the weight of the heat exchangers in the SOFC system increases. This could be due to the fact that at so high pressure requires havier and thicker tube in the heat exchangers to resist at those stresses. Indeed, the increase in weight concerns the heat exchangers of the SOFC system, which have to deal with higher pressure than that inside the heat exchangers of the hydrogen release system.

The weight increase of the compressor, instead, is justified by the overall weight reduction of the heat exchangers. Indeed, considering the best case which is the one with a pressure of fluids equal to 1.95 bar, the weight of the compressor increases of about 115 kg, against a reduction of the heat exchangers weight of about 4700 kg.

The evolution of the weight of each subsystem and of the overall system is represented in Table 24.

Pressure [bar]	1.6	1.8	1.9	1.95	2
H2 RELEASE SYSTEM [kg]	17070	16485	16432	16326	16167
SOFC SYSTEM [kg]	19382	15896	15619	15544	17004
GLOBAL SYSTEM [kg]	36452	32381	32051	31870	33171

Table 24 Weight of each subsystem and of the overall system as a function of the pressurization

From a weight point of view, the best case is guaranteed by a pressure of 1.95 bar and characterized by 4582 kg saved with respect to the starting configuration.

As said at the beginning, this sensitivity analysis is done to decrease as much as possible the weight of the heat exchangers, which are the most impacting devices on the overall weight. Thanks to the pressurization, the impact of the heat exchangers is decreased and the results are listed in the following table.

Pressure [bar]	1.6	1.8	1.9	1.95	2
HEX [%]	50.65	44.23	43.56	43.19	45.36

Table 25 Impact decrease on the overall system of the heat exchangers as a function of the pressurization

Therefore, by increasing the pressure, it is possible to decrease the impact of the heat exchangers by about 7%, considering the best case, thus characterized by a p = 1.95 bar.

Right now, for a pressure equal to 1.95 bar, a FU equal to 0.85 and a pressure drop in each heat exchanger of 0.14 bar, the impact of each component on the overall system is the following:

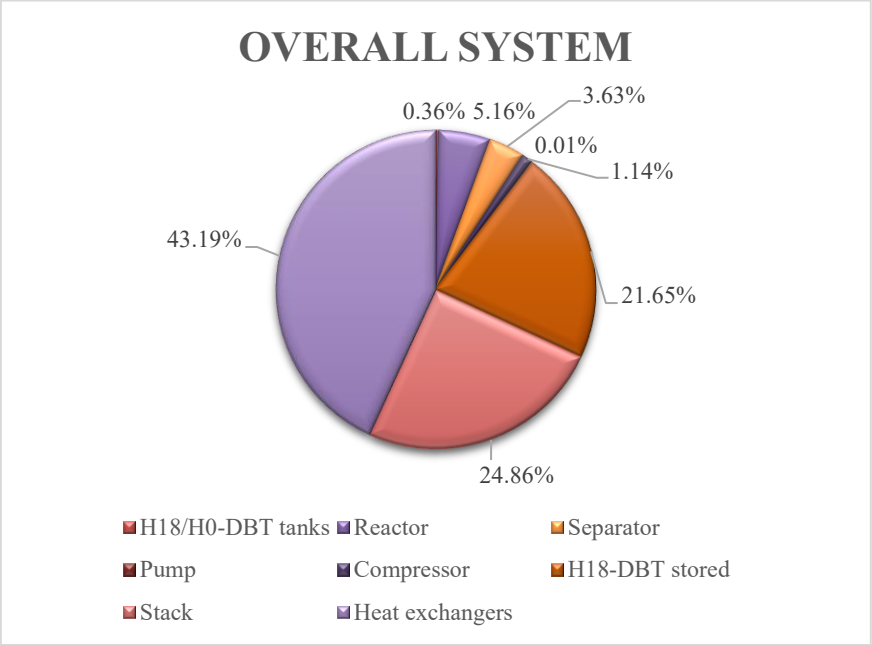

Figure 31 Weight impact of each component on the overall system for a pressurization p=1.95 bar

Finally, the gravimetric index of the storage system is positively affected by the pressurization. The results are listed in the following table:

Pressure [bar]	1.6	1.8	1.9	1.95	2
wt%H2	2.41	2.49	2.50	2.52	2.54

Table 26 Grvimetric index of the H_2 storage system for different pressurizations

From the gravimetric index point of view the best case is represented by a pressure equal to 2 bar, while from the weight point of view the best case is achieved for a pressure of 1.95 bar. This is explained by the fact that the weight increase for a pressure of 2 bar, is related to heat exchangers in the SOFC system which are not considered in the evaluation of the gravimetric index. However, the most important aspect on the feasibility of the system is the weight, thus the best configuration is represented by a pressure of the fluids equal to 1.95 bar.

To further decrease the weight of the system, another option is to increase the pressure drop to 0.34 bar. In the next chapter, the best configuration achieved so far will be studied under different pressure drops.

7.3. PRESSURE DROP INSIDE THE HEAT EXCHANGERS

As can be seen in Figure 31, the impact of the heat exchangers accounts the 43.19%. Thus, to decrease their weight the pressure drop across each heat exchanger is increased, to enhance the turbulence of the streams and to improve the heat transfer. The pressure drop is increased from 0.14 to 0.34 bar and not beyond, to avoid a subatmospheric pressure inside the last heat exchanger (HEX-LOHC).

The results obtained are:

Δp [bar]	**0.14**	**0.34**
Hex-H_2 release system [kg]	6508	4330
Hex-SOFC system [kg]	7256	6929
Hex-TOT [kg]	13764	11259

Table 27 Weight reduction of the heat exchangers for different pressure drops

As can be seen in Table 27, increasing the pressure drop is possible to save a lot of weight. Indeed, through this method the total weight of the heat exchangers is reduced by 2500 kg. Consequently, their impact on the overall system will decrease and the results are listed in Table 28.

Δp [bar]	**0.14**	**0.34**
HEX [%]	43.19	38.34

Table 28 Impact reduction of the heat exchangers on the overall system for different pressure drops

Thus, considering a pressure drop of 0.34 bar the impact of the heat exchangers on the overall system decreases by about 5%.

Concerning the weight of each subsystem and of the overall system, the results are summarized in the following table:

Δp [bar]	0.14	0.34
H2 RELEASE SYSTEM [kg]	16326	14148
SOFC SYSTEM [kg]	15544	15217
OVERALL SYSTEM [kg]	31870	29365

Table 29 Weight of each subsystem and of the overall system as a function of the pressure drop in the heat exchangers

The decrease of weight in the overall system is equal to the one of just the heat exchangers, since this sensitivity analysis regarded only the heat exchangers.

Concerning the impact of each component, in percentage terms, on the overall system, the situation can be visualized in the following pie chart:

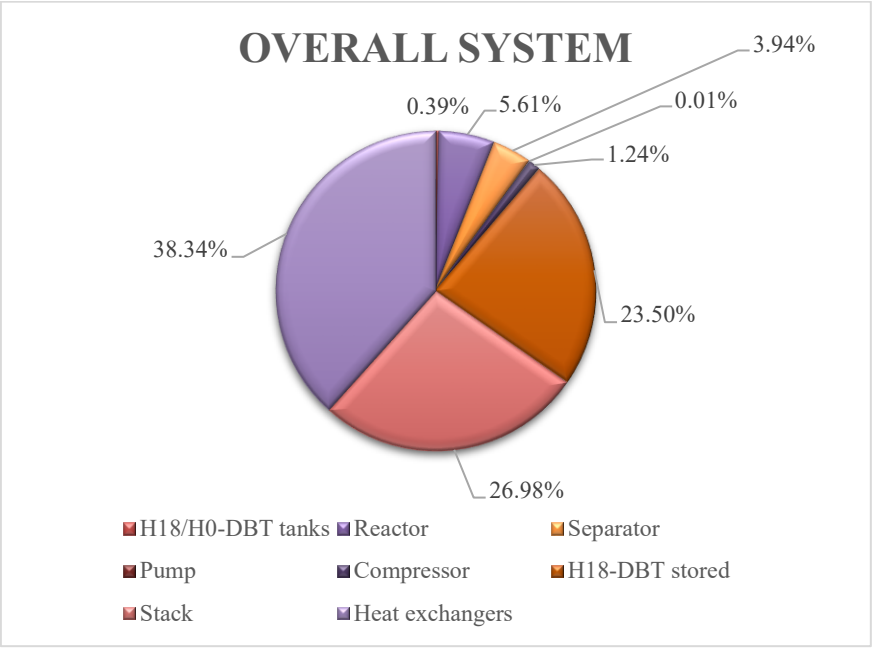

Figure 32 Impact of each component on the overall system for a pressure drop in the heat exchangers of 0.34 bar

Even in this case as happened in the previous sensitivity analsys, the gravimetric index is increased. The increase can be seen in the table below:

Delta P [bar]	0.14	0.34
wt%H2	2.52	2.90

Table 30 Gravimetric index of the H_2 storage system for different pressure drop in the heat exchangers

As can be seen, a decrease of 1200 kg in the heat exchangers belonging to the hydrogen release system, leads to increase the gravimetric index by 0.4%.

7.4. CONSIDERATIONS ON THE FINAL CONFIGURATION OF THE ALL-ELECTRIC CASE

The sensitivity analysis had the goal of decreasing the weight of the overall system as much as possible, to evaluate the fasibility of an all-electric ATR-72 600. In the following table the weight of the starting configuration and of the ones obtained through the sensitivity analysis are listed, to see the improvement:

	FU	FU	p [bar]	Δp [bar]
	0.7	0.85	1.95	0.34
H2 RELEASE SYSTEM [kg]	20355	17070	16326	14148
SOFC SYSTEM [kg]	20389	19382	15544	15217
OVERALL SYSTEM [kg]	40745	36452	31870	29365

Table 31 Comparison between the configuration of each sensitivity analysis

Starting from a configuration characterized by a FU = 0.7, a pressure of the fluid entering the SOFC stack equal to 1.6 bar, a pressure drops of the heat exchangers of 0.14 bar and an overall weight of 40745 kg, the sensitivity analysis end up with the best configuration "Δp = 0.34" characterized by a FU = 0.85, a pressure of the fluid entering the stack of 1.95 bar and an overall weight of 29365 kg.

Thus, the best configuration guaranteed a reduction of 11380 kg, with respect to the initial case study.

The reduction of weight can be visualized in the following chart:

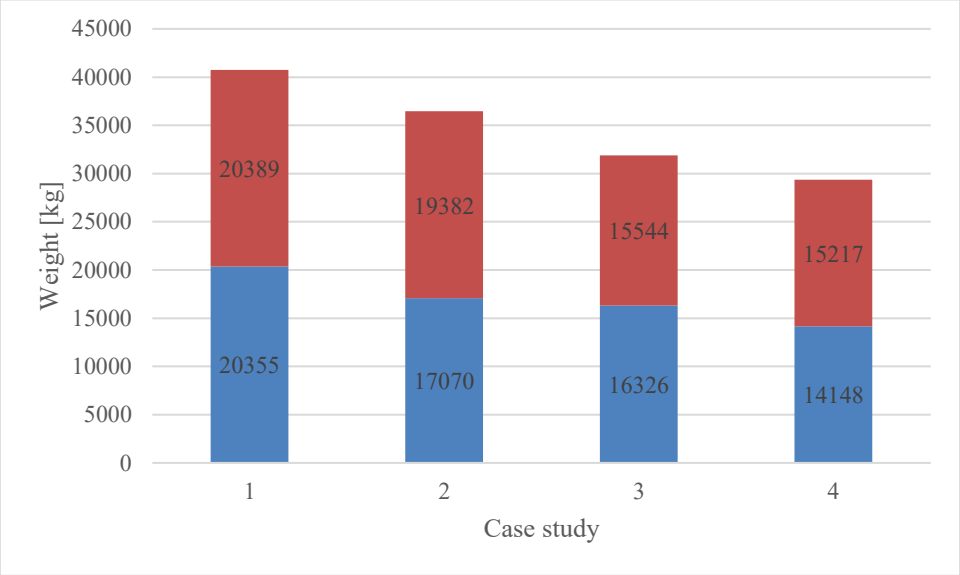

Figure 33 Weight reduction for each sensitivity analysis carried out

In Figure 33 Weight reduction for each sensitivity analysis carried outFigure 33, the cases are characterized as follow:

1. FU = 0.7, p = 1.6 bar and Δp = 0.14 bar;
2. FU = 0.85, p = 1.6 bar and Δp = 0.14 bar;
3. FU = 0.85, p = 1.95 bar and Δp = 0.14 bar;
4. FU = 0.85, p = 1.95 bar and Δp = 0.34 bar;

However, this weight reduction is not enough to allow the feasibility of an all-electric ATR-72 600. Remebering that the MTOW of the conventional ATR-72 600, the MTOW of the best configuration, found after the sensitivity analysis, is equal to 48446 kg. Thus, 25646 kg more than the conventional MTOW.

Even if the 72 passengers were removed, the plane would still be too heavy. Indeed, to allow the feasibility of the all-electric case, the number of passengers to be removed should be 318 making impossible to achieve this requirement.

To better visualize the difference between the conventional and all-electric case the following chart can be used:

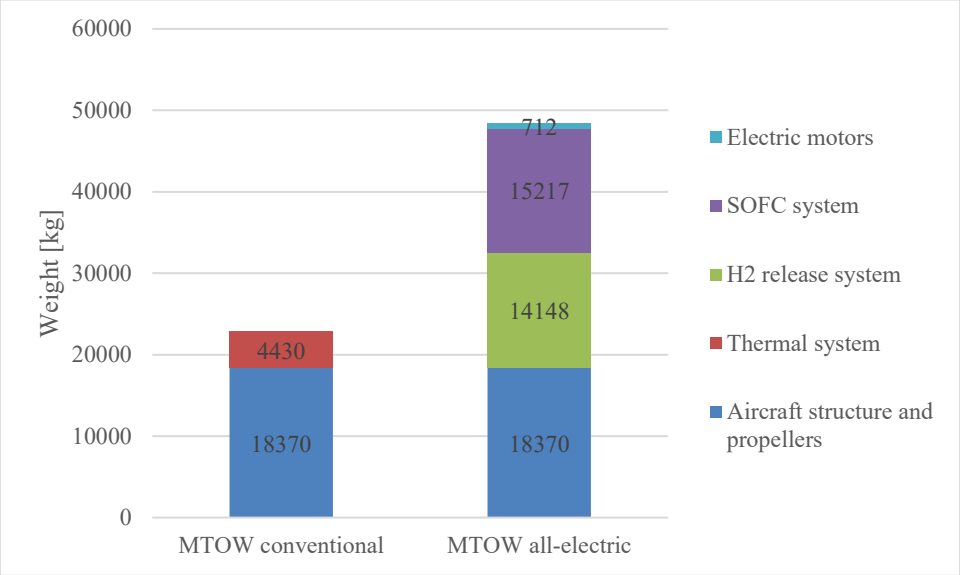

Figure 34 Comparison between the conventional and the best configuration of the all-electric MTOW

At this point, whereas a fully electric case is not feasible, different degrees of hybridization of the system will be studied. In this way, the feasibility of a hybrid system that provides at least a reduction in greenhouse gas emissions will be pursued.

8. HYBRIDIZATION OF THE ATR-72 600

In this chapter, four degrees of hybridization will be studied and they are the 80,60,40 and 20% of the conventional configuration. The goal is to evaluate the feasibility of at least one degree of hybridization. If more cases are feasible, the one with the highest grade will be considered. The characteristics of the system are: FU = 0.85, pressure of fluid entering the stack equal to 1.95 bar and a pressure drop of the heat exchangers of 0.34 bar.

8.1. 80% OF HYBRIDIZATION

To have an 80% of hybridization the SOFC stack should be able to provide 2.96 MW of electrical power. To do so, the mass flow rates of H18-DBT and H_2 are listed in the following table, including their respective stored masses:

H2 flow [kg/s]	0.037
H2 stored [kg]	328.52
H18-DBT flow [kg/s]	0.619
H18-DBT stored	5520

Table 32 H18-DBT and H_2 stored and mass flow rate for 80% of hybridization

Once this set of data is known, the procedure used in chapter 6.2 for the weight evaluation of each component is applied even in this case. The weight characterizing the hydrogen release system are listed in Table 33.

	Weight [kg]
H18-DBT tank	44.70
H0-DBT tank	47.94
Reactor	1320
Separator	841.43
Pump	1.92
Hex-LOHC	1713
COOL	1713

Table 33 Weight of each component of the H_2 release system for 80% of hybridization

Instead, concerning the weight related to the SOFC systems, they are:

	Weight [kg]
Compressor	291.9
SOFC stack	6338
Hex-H_2	3041
Hex-AIR	2431

Table 34 Weight of each component of the SOFC system for 80% of hybridization

Finally, the total weight of each subsystem and of the overall system is computed:

	Weight [kg]
H_2 RELEASE SYSTEM	11202
SOFC SYSTEM	12102
OVERALL SYSTEM	23304

Table 35 Weight of each subsystem and of the overall system for 80% of hybridization

For this degree of hybridization, the impact of each component on the overall system is:

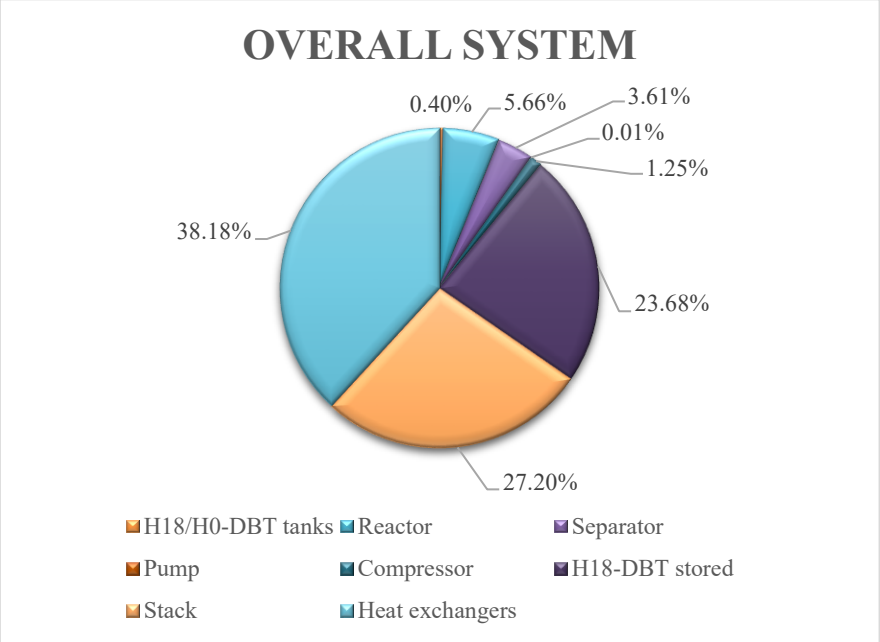

Figure 35 Weight impact of each component in percentage terms on the overall system for 80% of hybridization

As can be seen, the major contribution is always related to the heat exchangers. To reduce their weight a more efficient type of heat exchanger should be used. Concerning the amount of H18-DBT stored, its weight cannot be further decreased since its capacity of hydrogen storage is 6.2 wt%. The weight of the stack, it can be decreased choosing another type of SOFC characterized by a higher power density.

The gravimetric index of this configuration is equal to 2.93%, thus 0.03% higher than the best configuration of the all-elelctric case. In addition to the general decrease in weights, this could be explained by the fact that in the all-electric case the weight separator is not scaled according to the improvements, remaining constant. Instead, with this degree of hybridization the weight of the separator is diminished and thus it could have a size more correlated to the mass flow rates flowing within the system.

8.1.1. FEASIBILITY EVALUATION OF THE 80% HYBRIDIZATION CASE

To evaluate the feasibility of this configuration, it must be added to the the overall system weight computed in Table 35, the contribution of the conventional propulsion system. Indeed, the 80% is represented by the H_2 release system, the SOFC system and the electric motors, while the remaining 20% includes the conventional propulsion system, thus the keorsene system. The conventional propulsion will be scaled according to the degree of hybridization. Considering that the thermal system includes the fuel, the kerosene system and two thermal engines its weight is 4430 kg. Therefore, due to the hydridization, the weight to consider is the 20% of the total, which is equal to 886 kg. The MTOW of this hybridized configuration is 43129 kg. To allow the the feasibility of the aircraft, it should weight 20329 kg less, thus even this configuration is not feasible. To allow the feasibility of the aircraft, in terms of passengers that have to be removed, they should be 267 less.

The comparison between the conventional and hybrid MTOW can be seen in the following chart:

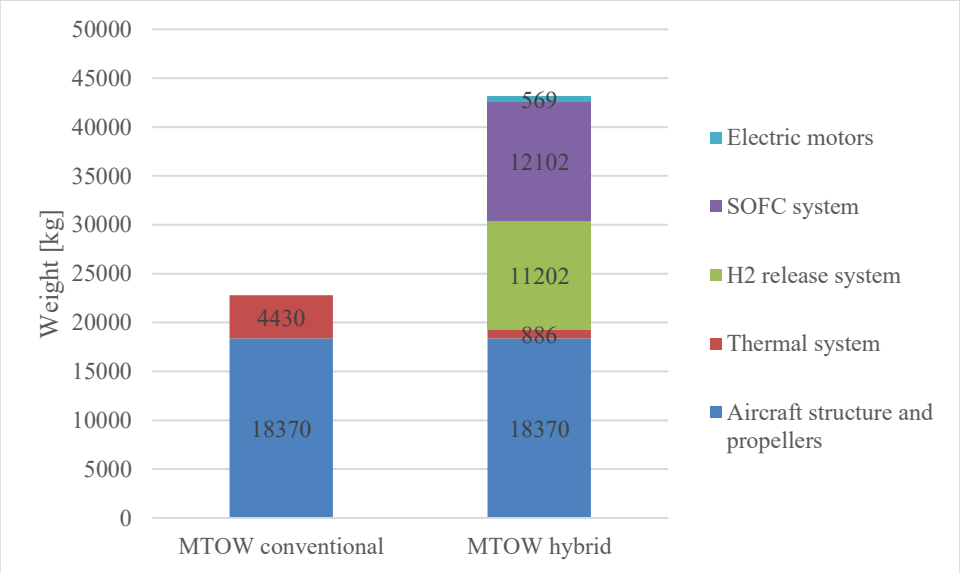

Figure 36 Comparison between the conventional and the MTOW for a HD = 80%

8.2. 60% OF HYBRIDIZATION

Having a 60% of hybridization means to supply 2.22 MW through the SOFC stack. To do so, the mass flow rate and the amount of H18-DBT and H_2 stored are:

H2 flow [kg/s]	0.028
H2 stored [kg]	244.18
H18-DBT flow [kg/s]	0.46
H18-DBT stored [kg]	4102

Table 36 H18-DBT and H_2 stored and mass flow rate for 60% of hybridization

Cosnequently the weight characterizing each component of the H_2 release system are summarized in Table 37.

	Weight [kg]
H18-DBT tank	34.29
H0-DBT tank	36.70
Reactor	984.55
Separator	714.41
Pump	1.43
Hex-LOHC	970.5
COOL	970.5

Table 37 Weight of each component of the H_2 release system for 60% of hybridization

At the same time the weight of the components related to the SOFC system are:

	Weight [kg]
Compressor	216.96
SOFC stack	4754
Hex-H2	1607
Hex-AIR	2138

Table 38 Weight of each component of the SOFC system for 60% of hybridization

Once the weight of each component is known, the overall weight is calculated and the results are listed in the following table:

	Weight [kg]
H2 RELEASE SYSTEM	7815
SOFC SYSTEM	8716
OVERALL SYSTEM	16531

Table 39 Weight of each subsystem and of the overall system for 60% of hybridization

To know the percentage represented by each component concerning the overall system, the following pie chart is considered:

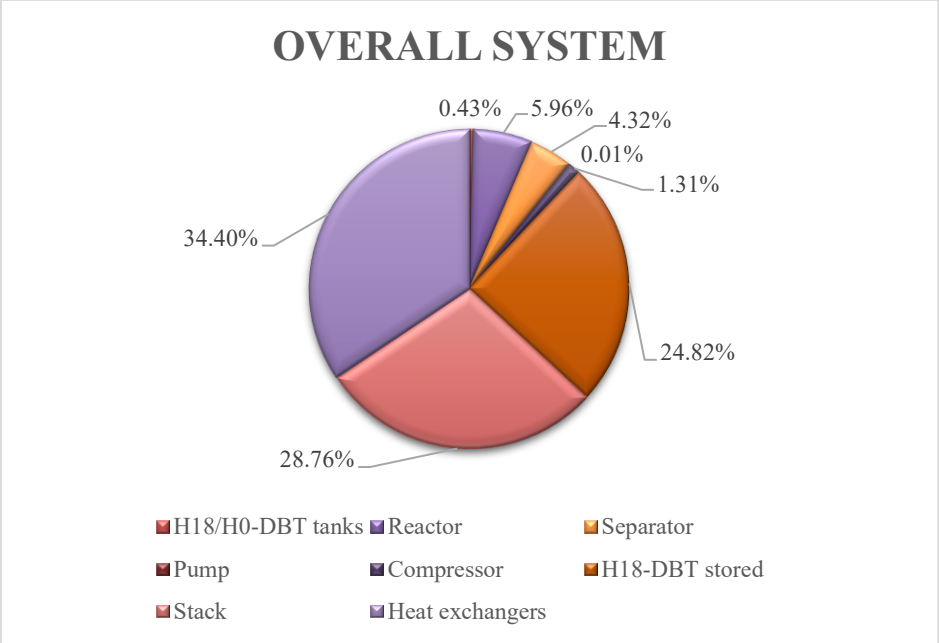

Figure 37 Weight impact of each component in percentage terms on the overall system for 60% of hybridization

In this configuration, the impact of the heat exchangers is lower than the case with a degree of hybridization equal to 80 %. This could be explained by the lower mass flow rate within the system, that has a major impact on these components and by the increase in terms of percentage of the separator. Indeed, the separator percentage has increased of about 1%. This is explained by the fact that,

considering the mass flow rates within the system the separator should have a size of 36”x15’, but in reference [37] the weight related to that size is not reported. Therefore, the weight of the separator is approximated for excess to the weight of a separator with size equal to 42”x10’.

The gravimetric index of this configuration is equal to 3.12%, thus it is increased of the 0.19% with respect to the previous case.

8.2.1. FEASIBILITY EVALUATION OF THE 60% HYBRIDIZATION CASE

As explained in chapter 8.1.1, to evaluate the feasibility of the system, the contribution of the electric and conventional system has to be considered. Thus, the MTOW characterizing this configuration will be equal to 37100 kg, where the contribution of the electric system is 16958 kg and the one of the thermal system is 1772 kg. The remaining part is related to the weight of the aircraft structures and propellers.

Remembering that the MTOW of the conventional ATR-72 600 is 22800 kg, this configuration is not feasible, being characterized by a MTOW of 37100 kg. Even removing the 72 passangers, would not be possible to fly since the number of passengers to be removed is 210.

Even in this case a chart is used to visualize the difference between the conventional and hybridized MTOW:

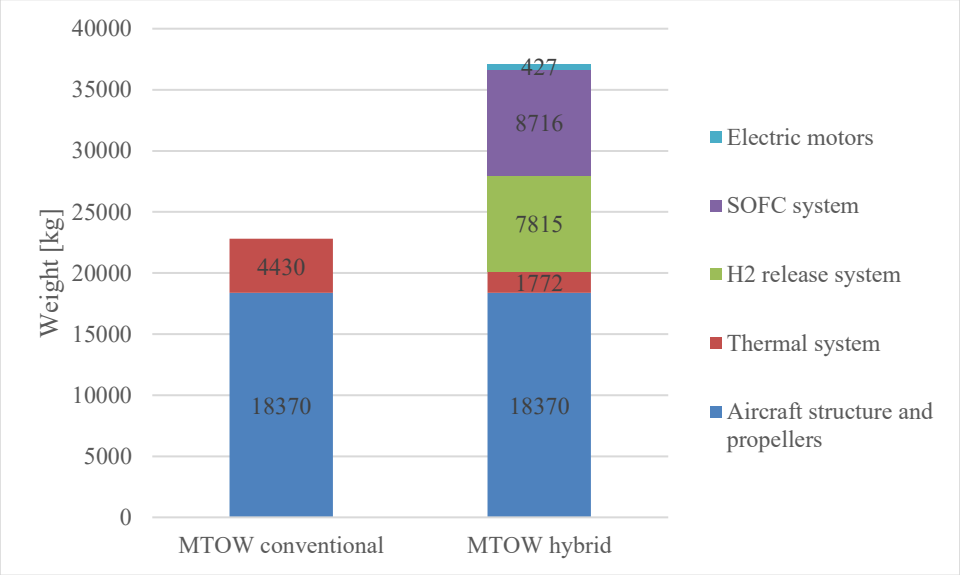

Figure 38 Comparison between the conventional and the MTOW for a HD = 60%

8.3. 40% IBRIDIZATION

In case of a degree of hybridization equal to 40%, the SOFC stack should be able to provide 1.48 MW of electrical power. To guarantee this amount of power, the following conditions are necessary:

H2 flow [kg/s]	0.019
H2 stored [kg]	164.27
H18-DBT flow [kg/s]	0.31
H18-DBT stored [kg]	2760

Table 40 H18-DBT and H_2 stored and mass flow rate for 40% of hybridization

Then, the weight of each component related to the H2 release and SOFC system is listed in Table 41 and Table 42, respectively:

	Weight [kg]
H18-DBT tank	24.43
H0-DBT tank	26.05
Reactor	667.43
Separator	578.34
Pump	0.96
Hex-LOHC	591.5
COOL	591.5

Table 41 Weight of each component of the H_2 release system for 40% of hybridization

	Weight [kg]
Compressor	145.95
SOFC stack	3169
Hex-H2	1424
Hex-AIR	988.6

Table 42 Weight of each component of the SOFC system for 40% of hybridization

Finally, the weight of the susbsytems and of the overall system is:

	Weight [kg]
H2 RELEASE SYSTEM	5240
SOFC SYSTEM	5728
OVERALL SYSTEM	10968

Table 43 Weight of each subsystem and of the overall system for 40% of hybridization

Even in this case, the impact of each component on the overall system can be visualized in the following pie chart:

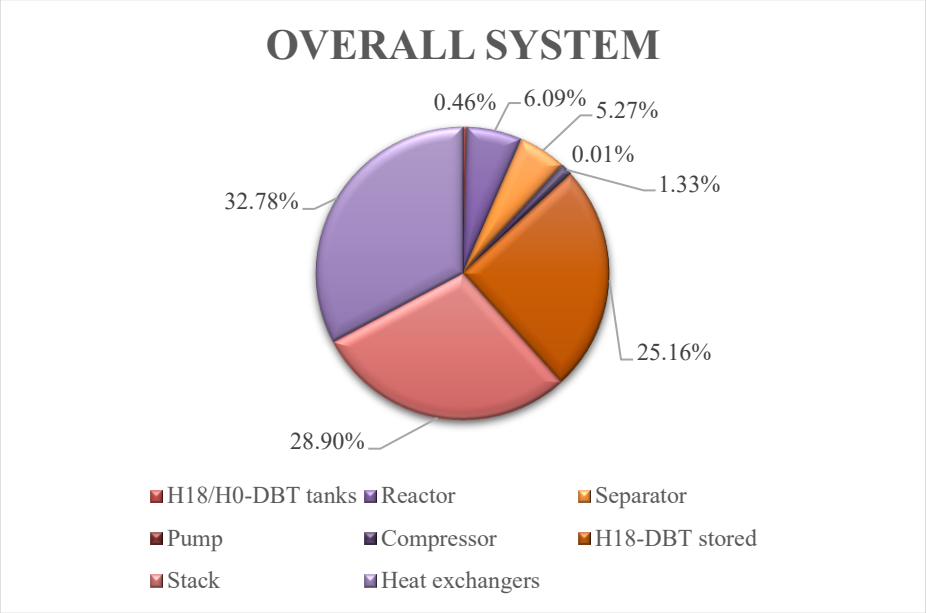

Figure 39 Weight impact of each component in percentage terms on the overall system for 40% of hybridization

Looking at the pie chart, the heat exchangers account for the 32.78% of the overall system weight, that is slightly lower than the system with a hybridization degree equal to 60%. The reason why this happens, could be due to the lower mass flow rates within the systems.

Concerning the gravimetric index of the H_2 storage system, it is increased up to the 3.13%, against the 3.12% of the previous configuration. Thus, it is not so significant as increasing.

8.3.1. FEASIBILITY EVALUATION OF THE 40% HYBRIDIZATION CASE

In case of a 40% hybridization, the MTOW is 32280 kg, where the electric system contributes with 11252 kg, the thermal system contributes with 2658 kg and the remaining part, as always, is related to the aircraft structure and propellers.

However, even with this solution the aircraft is not able to fly because of the excessive weight. Indeed, the excess of weight is equal to 9480 kg concerning the minimum required. Even after the 72 passengers' removal, this configuration is not feasible since the number of passengers to be removed is 163.

To better analyze the comparison between the conventional and hybridized MTOW the following picture is used:

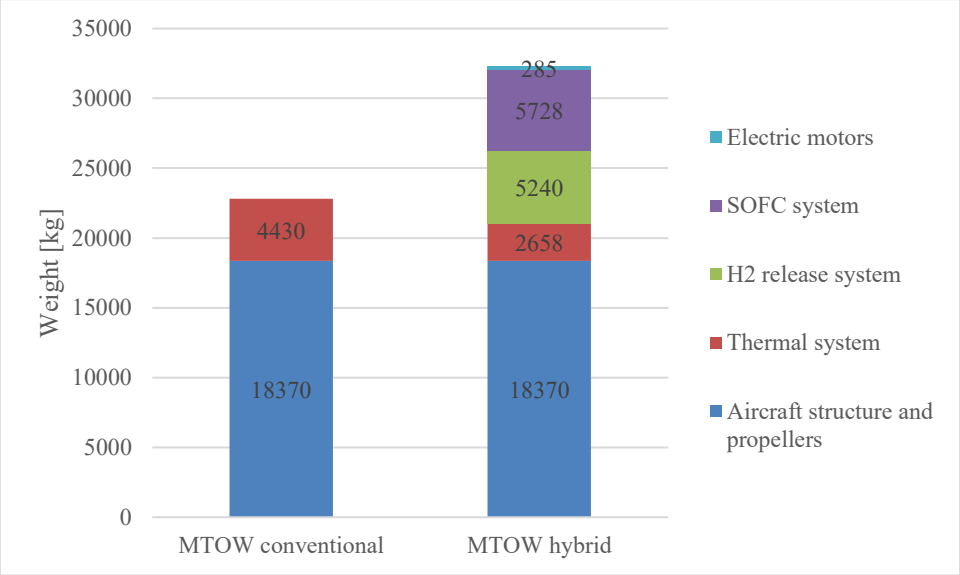

Figure 40 Comparison between the conventional and the MTOW for an HD = 40%

8.4. 20% IBRIDIZATION

For a degree of hybridization equal to 20%, the SOFC stack must supply 680 kW of electrical power. To supply such power, the required mass flow rates and masses to be stored are the following:

H2 flow [kg/s]	0.009
H2 stored [kg]	75.49
H18-DBT flow [kg/s]	0.14
H18-DBT stored [kg]	1268

Table 44 H18-DBT and H_2 stored and mass flow rate for 20% of hybridization

Concerning the weight of each component included in the H_2 release system, they are listed in Table 45.

	Weight [kg]
H18-DBT tank	13.48
H0-DBT tank	14.22
Reactor	314.82
Separator	464.94
Pump	0.44
Hex-LOHC	163.8
COOL	163.8

Table 45 Weight of each component of the H_2 release system for 20% of hybridization

While the components of the SOFC system is characterized by the weight included in Table 46.

	Weight [kg]
Compressor	67.07
SOFC stack	1456
Hex-H2	355.7
Hex-AIR	377

Table 46 Weight of each component of the SOFC system for 20% of hybridization

After the evaluation of the weight of each component, the weight of the H_2 release, SOFC and overall system is computed:

	Weight [kg]
H2 RELEASE SYSTEM	2404
SOFC SYSTEM	2256
OVERALL SYSTEM	4660

Table 47 Weight of each subsystem and of the overall system for 20% of hybridization

Finally, thanks to the weight of each component and the one of the overall system, is possible to evaluate the percentage contribution of every component representing them in Figure 41:

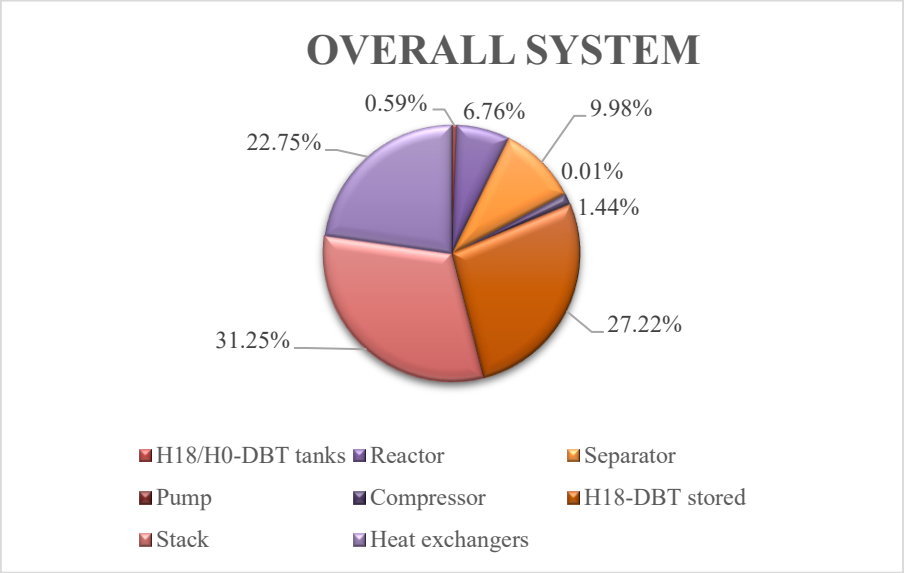

Figure 41 Weight impact of each component in percentage terms on the overall system for 20% of hybridization

8.4.1. FEASIBILITY EVAULATION OF THE 20% HYDBRIDIZATION CASE

As done for the previous hybridization case, the MTOW takes into account the weight of the electric and thermal system. Particularly, the electric system weights 4660 kg and the thermal one weight 3544 kg. Consdering the aircraft structure and the propellers, the MTOW is 26704 kg. Making a comparison with the MTOW of the conventional ATR-72 600, the one of the hybridized case is 3018 kg more. Thus, even with a degree of hybridization equal to 20%, the aircraft is not able to fly. To allow the feasibility of this configuration as a function of the number of passengers that must be removed, not only the 72 passengers must be removed but also other 37 passengeres should be considered, for a total of passengers removed equal to 109. Therefore, a number of passengers even higher than the amount that the aircraft is able to transport.

The analysis of the comparison between the conventional and hybrid MTOW can be done by using the following chart:

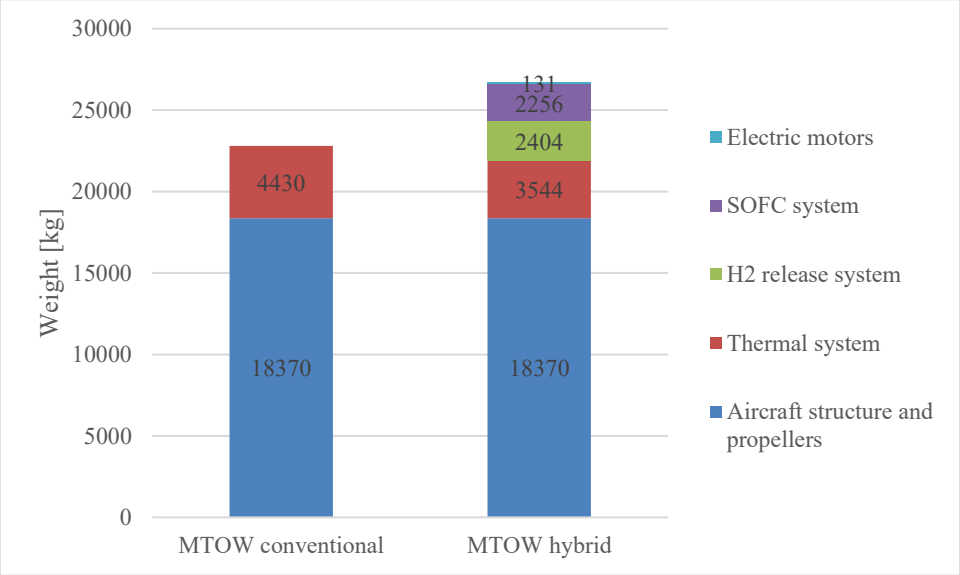

Figure 42 Comparison between the conventional and the MTOW for an HD = 20%

8.5. CONSIDERATIONS

Once alle the HD are evaluated, it is computed the evolution of the overall electric system weight (H_2 release and SOFC system) and the one of the MTOW, to find a sort of linearity. A HD lower than 20% is not considered, since the idea of this thesis was to find the feasibility of a system able to provide a significant contribution to the propulsion of the aircraft.

The data used for building the chart, in Figure 43, are listed in Table 48.

HD [%]	100	80	60	40	20
OVERALL SYSTEM [kg]	31870	23304	16531	10968	4660
MTOW [kg]	48446	43129	37100	32280	26704

Table 48 Weight of the overall system and of the MTOW as a function of the HD

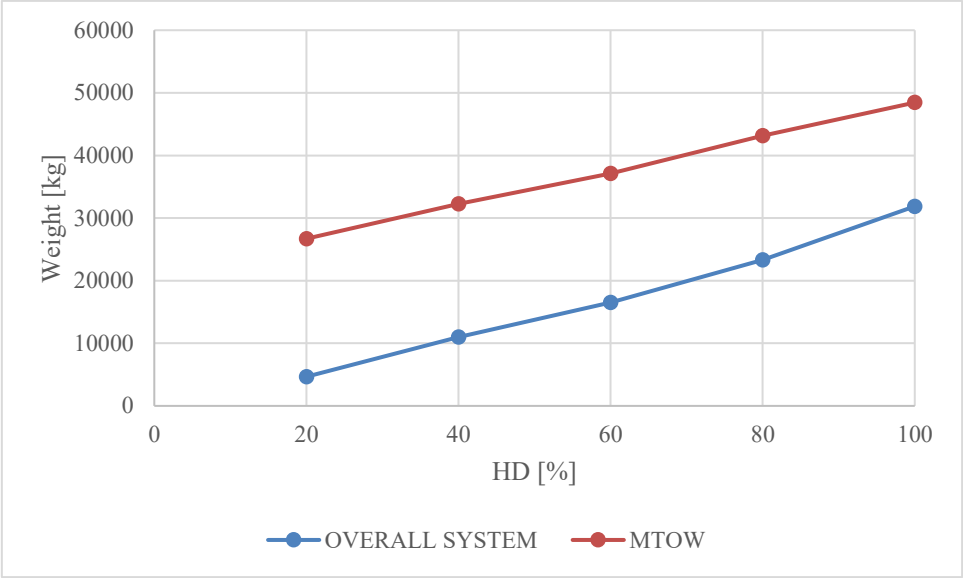

Figure 43 Evolution of the overall system and MTOW weight as a function of the HD

As can be seen, a sort of linearity is found. This is a quite interesting result, since it allows to evaluate, as a first approximation, the weight of the overall system or of the MTOW without calculating the weight of each component.

Unfortunately, there is any HD that allow the feasibility of a hybrid aircraft. Therefore, in the next chapter will be evaluated a future prospect considering technologies not yet commercialized that could allow the feasibility of a hybrid ATR-72 600.

9. FUTURE PROSPECTS

Sadly, with the nowadays technologies, a hybrid ATR-72 600 using a LOHC-SOFC technology is not feasible. Therefore, considering the components having major impact on the overall system weight which are the heat exchangers and the SOFC stack, as can be seen in Figure 42, new technologies best performing will be used. Considering the H18-DBT is not considered because no studies are found on the gravimetric index improvement.

The new SOFC technology is the so called thin-film SOFC that could achieve a power density equal to 2.58 kW/kg [39]. Concerning the new type of heat exchangers that could be used, it is an ultra power dense heat exchanger [43]. This heat exchanger is characterized by a tube-in-tube architecture designed through a genetic algorithm design and metal additive manufacturing. In this way, Moon and Co. [43] demonstrated a power density of the heat exchanger equal to 15.7 kW/kg.

These two technologies are used to evaluate the feasibility of the ATR-72 600 with a HD equal to the 20%.

The result obtained, in terms of weight are the following:

	Weight [kg]		
	H_2 release system	SOFC system	Overall system
Commercial technology	2404	2256	4660
Future technology	2091	394	2484

Table 49 Comparison in terms of weight between commercial and future technology

The reason why, the SOFC system experience a larger weight reduction is due to the fact that it is composed by the stack and heat exchangers, apart the compressor, which are both improved. In the H_2 release system instead, there are a lot of components, therefore the weight experiences a lower reduction. However, thanks to these technologies the overall weight has decreased by about 2200 kg.

Considering the impact of each component on the overall system, it is represented in Figure 44.

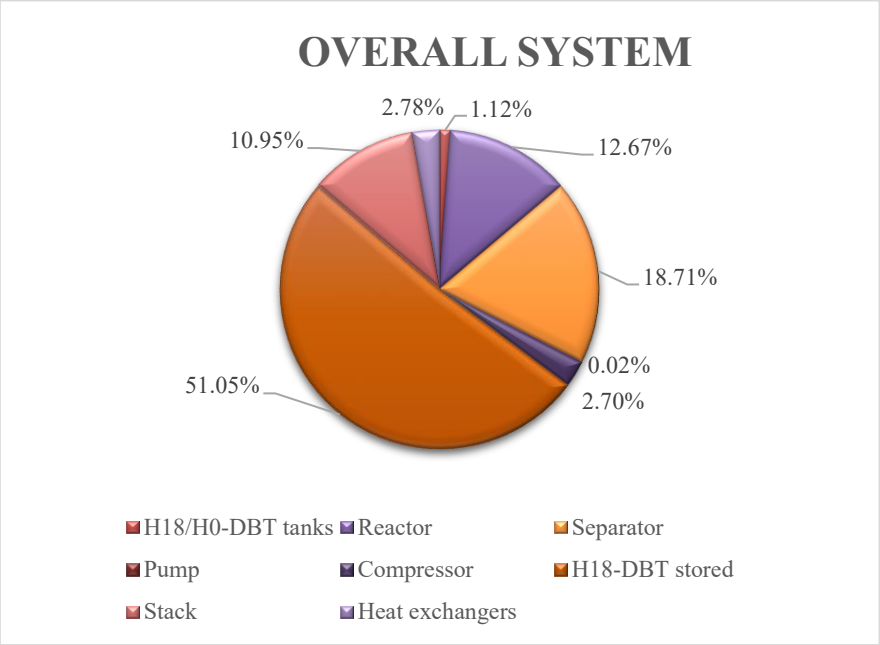

Figure 44 Weight impact of each component in percentage terms on the overall system using sperimental technology

Obviously, with respect to Figure 41, the impact of heat exchangers and of the SOFC stack has singnificantly reduced, while the mass of H18-DBT witouth being improved is become the most impacting weight on the overall system.

9.1. EVALUATION OF THE FEASIBILITY USING EXPERIMENTAL TECHNOLOGIES

Unfortunately, even after the use of experimental technology the 20% hybridization of the ATR-72 600 is not feasible. Indeed, the MTOW of the hybrid aircraft is 24529 kg, thus higher than the minimum required. Reasoning in terms of passengers that should be removed, the removal of 89 passengers is needed to allow the feasibility.

Making as always, the comparison between the conventional and hybrid MTOW, the results are displayed in the following chart:

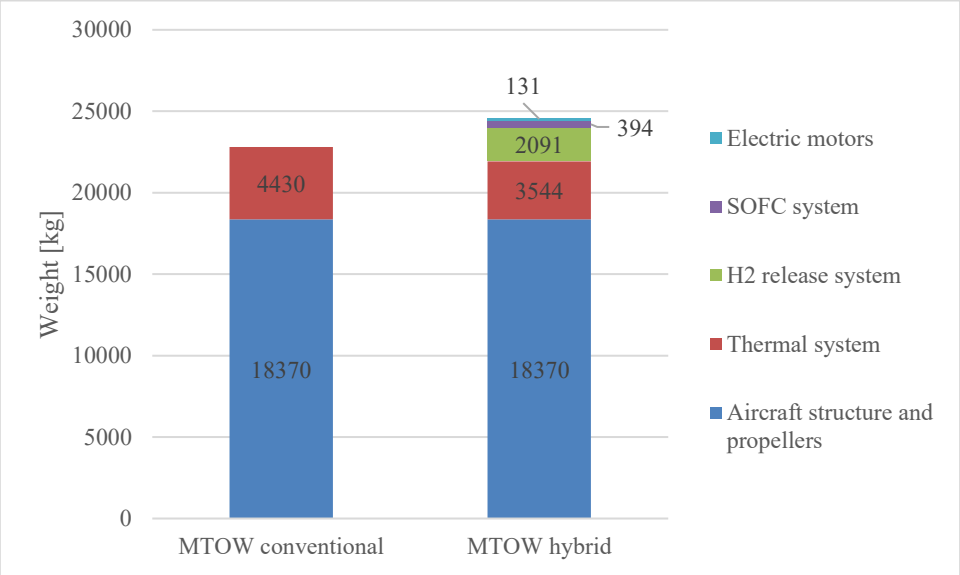

Figure 45 Comparison between the conventional and the MTOW for an HD = 20% using experimental technologies

Whereas a 20% HD is not feasible, the larger HD are not evaluated.

10. GRAVIMETRIC INDEX COMPARISON BETWEEN LOHC AND LH_2

In this chapter, a comparison between the LOHC and LH_2 is evaluated in order to study the competivity of a LOHC hydrogen storage technology in aircraft application. Indeed, the reason why it is compared with the LH_2 storage, is that the latter is the most used hydrogen technology used in the aviation field.

Considering the gravimetric index of the LOHC as can be seen in the various analysis made in this thesis, ranging from 2.45 to 3.14%, in case of hybridization. At the same time a reasonable gravimetric index of the LH_2 is 7.5%. Therefore, the LOHC technology because of the BoP is not so much competitive.

11. CONCLUSIONS

The aim of this thesis was to evaluate the feasibility of the ATR-72 600 electrification, by the coupling between a hydrogen storage technology and a fuel cell system. To do so, firstly a research from the literuature on the charatcteristics of the different hydrogen storage and fuel cell technologies has been carried out, to find the most promising technology to be used in aircraft applications. Thus, considering the interest in low TRL technologies, as hydrogen storage the LOHC technology has been chosen. At the sime time, the SOFC is selected to be coupled with the LOHC technology to provide the heat necessary for pre heating the streams of the system, thanks to the exhaust gas temperature.

Once these two technologies were coupled, the all-electric case was studied. Therefore, the weight of the overall system has been computed, by evaluating the weight of each component. Knowing the overall system weight, the MTOW was calculated to evaluate the feasibility of the all-electric ATR-72 600. Unfortunately, the system has proved to be unfeasible. Consequently, a sensitivity analysis on the FU, on the pressurization of the fluid entering the stack and on the pressure drop of the heat exchangers has been carried out. However, even in this case, the all-electric propulsion is not feasible.

At that point a hybridization of the conventional system has been performed, to check at least the feasibility of a hybrid system. Thus, four HD were evaluated: 80,60,40 and 20%. Among all the cases, even this time no system proved to be feasible. As last attempt, the 20% HD has been chosen to study using experimental technologies such as thin-film SOFC and ultra power dense heat exchangers, without obtaining the feasibility of the system.

In the future to allow the feasibility of the 20% of HD, the gravimetric index of the overall system, including only the H_2 release and SOFC system, should reach values equal to 10.78%, while the HD = 20% using experimental technologies is

equal to 2.94 %. Anyway, even considering a gravimetric index of 10.78% no passenger is allowed to fly, otherwise the weight would be too much.

BIBLIOGRAPHY

[1] "Azioni dell'UE per ridurre le emissioni di navi e aerei," *https://www.europarl.europa.eu/news/it/headlines/society/20220610STO32720/azioni-dell-ue-per-ridurre-le-emissioni-di-navi-e-aerei*.

[2] E. Rivard, M. Trudeau, and K. Zaghib, "Hydrogen storage for mobility: A review," *Materials*, vol. 12, no. 12. MDPI AG, Jun. 01, 2019. doi: 10.3390/ma12121973.

[3] A. G. Rao, F. Yin, and H. G. C. Werij, "Energy transition in aviation: The role of cryogenic fuels," *Aerospace*, vol. 7, no. 12. MDPI AG, pp. 1–24, Dec. 01, 2020. doi: 10.3390/aerospace7120181.

[4] C. Winnefeld, T. Kadyk, B. Bensmann, U. Krewer, and R. Hanke-Rauschenbach, "Modelling and designing cryogenic hydrogen tanks for future aircraft applications," *Energies (Basel)*, vol. 11, no. 1, Jan. 2018, doi: 10.3390/en11010105.

[5] P. T. Aakko-Saksa, C. Cook, J. Kiviaho, and T. Repo, "Liquid organic hydrogen carriers for transportation and storing of renewable energy – Review and discussion," *Journal of Power Sources*, vol. 396. Elsevier B.V., pp. 803–823, Aug. 31, 2018. doi: 10.1016/j.jpowsour.2018.04.011.

[6] Y. Kwak *et al.*, "Hydrogen production from homocyclic liquid organic hydrogen carriers (LOHCs): Benchmarking studies and energy-economic analyses," *Energy Convers Manag*, vol. 239, Jul. 2021, doi: 10.1016/j.enconman.2021.114124.

[7] "The Chemistry Behind Metal Hydrides for Fuel Cells," *www.fuelcellstore.com*.

[8] M. Niermann, A. Beckendorff, M. Kaltschmitt, and K. Bonhoff, “Liquid Organic Hydrogen Carrier (LOHC) – Assessment based on chemical and economic properties,” *International Journal of Hydrogen Energy*, vol. 44, no. 13. Elsevier Ltd, pp. 6631–6654, Mar. 08, 2019. doi: 10.1016/j.ijhydene.2019.01.199.

[9] J. Geiling *et al.*, “Combined dynamic operation of PEM fuel cell and continuous dehydrogenation of perhydro-dibenzyltoluene,” *Int J Hydrogen Energy*, vol. 46, no. 72, pp. 35662–35677, Oct. 2021, doi: 10.1016/j.ijhydene.2021.08.034.

[10] A. Fikrt *et al.*, “Dynamic power supply by hydrogen bound to a liquid organic hydrogen carrier,” *Appl Energy*, vol. 194, pp. 1–8, 2017, doi: 10.1016/j.apenergy.2017.02.070.

[11] R. K. Ahluwalia, T. Q. Hua, and J. K. Peng, “Automotive storage of hydrogen in alane,” *Int J Hydrogen Energy*, vol. 34, no. 18, pp. 7731–7740, Sep. 2009, doi: 10.1016/j.ijhydene.2009.07.013.

[12] L. J. Bannenberg *et al.*, “Metal (boro-) hydrides for high energy density storage and relevant emerging technologies,” *Int J Hydrogen Energy*, vol. 45, no. 58, pp. 33687–33730, Nov. 2020, doi: 10.1016/j.ijhydene.2020.08.119.

[13] L. Wang, M. Z. Quadir, and K. F. Aguey-Zinsou, “Direct and reversible hydrogen storage of lithium hydride (LiH) nanoconfined in high surface area graphite,” *Int J Hydrogen Energy*, vol. 41, no. 40, pp. 18088–18094, Oct. 2016, doi: 10.1016/j.ijhydene.2016.07.073.

[14] S. Wang *et al.*, “A nanoconfined-LiBH4 system using a unique multifunctional porous scaffold of carbon wrapped ultrafine Fe3O4 skeleton for reversible hydrogen storage with high capacity,” *Chemical Engineering Journal*, vol. 428, Jan. 2022, doi: 10.1016/j.cej.2021.131056.

[15] H. ZHOU, H. zhen LIU, S. chao GAO, and X. hua WANG, “Enhanced dehydrogenation kinetic properties and hydrogen storage reversibility of

LiBH4 confined in activated charcoal," *Transactions of Nonferrous Metals Society of China (English Edition)*, vol. 28, no. 8, pp. 1618–1625, Aug. 2018, doi: 10.1016/S1003-6326(18)64804-6.

[16] H. Benzidi *et al.*, "Improved thermodynamic properties of doped LiBH4 for hydrogen storage: First-principal calculation," *Int J Hydrogen Energy*, vol. 44, no. 31, pp. 16793–16802, Jun. 2019, doi: 10.1016/j.ijhydene.2019.04.241.

[17] T. T. Le *et al.*, "Nanoconfinement effects on hydrogen storage properties of MgH2 and LiBH4," *International Journal of Hydrogen Energy*, vol. 46, no. 46. Elsevier Ltd, pp. 23723–23736, Jul. 06, 2021. doi: 10.1016/j.ijhydene.2021.04.150.

[18] M. Konarova, A. Tanksale, J. Norberto Beltramini, and G. Qing Lu, "Effects of nano-confinement on the hydrogen desorption properties of MgH2," *Nano Energy*, vol. 2, no. 1, pp. 98–104, Jan. 2013, doi: 10.1016/j.nanoen.2012.07.024.

[19] R. K. Ahluwalia, "Sodium alanate hydrogen storage system for automotive fuel cells," *Int J Hydrogen Energy*, vol. 32, no. 9, pp. 1251–1261, Jun. 2007, doi: 10.1016/j.ijhydene.2006.07.027.

[20] P. Brack, S. E. Dann, and K. G. Upul Wijayantha, "Heterogeneous and homogenous catalysts for hydrogen generation by hydrolysis of aqueous sodium borohydride (NaBH4) solutions," *Energy Science and Engineering*, vol. 3, no. 3. John Wiley and Sons Ltd, pp. 174–188, May 01, 2015. doi: 10.1002/ese3.67.

[21] Y. Kojima *et al.*, "Development of 10 kW-scale hydrogen generator using chemical hydride," *J Power Sources*, vol. 125, no. 1, pp. 22–26, Jan. 2004, doi: 10.1016/S0378-7753(03)00827-9.

[22] M. v. Lototskyy *et al.*, "Metal hydride systems for hydrogen storage and supply for stationary and automotive low temperature PEM fuel cell power

modules," in *International Journal of Hydrogen Energy*, Sep. 2015, vol. 40, no. 35, pp. 11491–11497. doi: 10.1016/j.ijhydene.2015.01.095.

[23] R. Peters *et al.*, "A solid oxide fuel cell operating on liquid organic hydrogen carrier-based hydrogen – A kinetic model of the hydrogen release unit and system performance," *Int J Hydrogen Energy*, vol. 44, no. 26, pp. 13794–13806, May 2019, doi: 10.1016/j.ijhydene.2019.03.220.

[24] R. Aslam, M. Minceva, K. Müller, and W. Arlt, "Development of a liquid chromatographic method for the separation of a liquid organic hydrogen carrier mixture," *Sep Purif Technol*, vol. 163, pp. 140–144, May 2016, doi: 10.1016/j.seppur.2016.01.051.

[25] S. Lee, G. Han, T. Kim, Y. S. Yoo, S. Y. Jeon, and J. Bae, "Connected evaluation of polymer electrolyte membrane fuel cell with dehydrogenation reactor of liquid organic hydrogen carrier," *Int J Hydrogen Energy*, vol. 45, no. 24, pp. 13398–13405, May 2020, doi: 10.1016/j.ijhydene.2020.02.129.

[26] A. Baroutaji, T. Wilberforce, M. Ramadan, and A. G. Olabi, "Comprehensive investigation on hydrogen and fuel cell technology in the aviation and aerospace sectors," *Renewable and Sustainable Energy Reviews*, vol. 106, pp. 31–40, May 2019, doi: 10.1016/j.rser.2019.02.022.

[27] R. E. Rosli *et al.*, "A review of high-temperature proton exchange membrane fuel cell (HT-PEMFC) system," *Int J Hydrogen Energy*, vol. 42, no. 14, pp. 9293–9314, Apr. 2017, doi: 10.1016/j.ijhydene.2016.06.211.

[28] "Proton-exchange membrane fuel cell," *https://en.wikipedia.org/wiki/Proton-exchange_membrane_fuel_cell*.

[29] Massimo Santarelli, "CELLE A COMBUSTIBILE A MEMBRANA POLIMERICA. DESCRIZIONE GENERALE DELLA CELLA E DEI SUOI PRINCIPI DI FUNZIONAMENTO".

[30] Q. Yan, H. Toghiani, and H. Causey, "Steady state and dynamic performance of proton exchange membrane fuel cells (PEMFCs) under

various operating conditions and load changes," *J Power Sources*, vol. 161, no. 1, pp. 492–502, Oct. 2006, doi: 10.1016/j.jpowsour.2006.03.077.

[31] A. Rabbani and M. Rokni, "Dynamic characteristics of an automotive fuel cell system for transitory load changes," *Sustainable Energy Technologies and Assessments*, vol. 1, no. 1, pp. 34–43, 2013, doi: 10.1016/j.seta.2012.12.003.

[32] "Solid oxide fuel cell," *https://en.wikipedia.org/wiki/Solid_oxide_fuel_cell*.

[33] Y. Bae, S. Lee, K. J. Yoon, J. H. Lee, and J. Hong, "Three-dimensional dynamic modeling and transport analysis of solid oxide fuel cells under electrical load change," *Energy Convers Manag*, vol. 165, pp. 405–418, Jun. 2018, doi: 10.1016/j.enconman.2018.03.064.

[34] Y. Qi, B. Huang, and J. Luo, "Dynamic modeling of a finite volume of solid oxide fuel cell: The effect of transport dynamics," *Chem Eng Sci*, vol. 61, no. 18, pp. 6057–6076, Sep. 2006, doi: 10.1016/j.ces.2006.05.030.

[35] G. Daniel. Brewer, *Hydrogen aircraft technology*. CRC Press, 1991.

[36] C. R. Sivalls, "OIL AND GAS SEPARATION DESIGN MANUAL," 2009.

[37] "Two Phase Low Pressure Horizontal Separators with Nominal Liquid and Gas Capacities," *https://umcenergy.com/two-phase-low-pressure-horizontal-separators-with-nominal-liquid-and-gas-capacities/*.

[38] C. J. Steffen, J. E. Freeh, and L. M. Larosiliere, "Solid Oxide Fuel Cell/Gas Turbine Hybrid Cycle Technology for Auxiliary Aerospace Power," 2005. [Online]. Available: http://www.sti.nasa.gov

[39] N. Q. Minh, "Solid Oxide Fuel Cell (SOFC) Technology For Powering the U.S. Army of the Future," 2020.

[40] M. Schröder, F. Becker, J. Kallo, and C. Gentner, "Optimal operating conditions of PEM fuel cells in commercial aircraft," *Int J Hydrogen*

Energy, vol. 46, no. 66, pp. 33218–33240, Sep. 2021, doi: 10.1016/j.ijhydene.2021.07.099.

[41] "STANDARD CONFIGURATION 72 seats."

[42] T. Kadyk, C. Winnefeld, R. Hanke-Rauschenbach, and U. Krewer, "Analysis and Design of Fuel Cell Systems for Aviation," *Energies (Basel)*, vol. 11, no. 2, Feb. 2018, doi: 10.3390/en11020375.

[43] H. Moon, D. J. McGregor, N. Miljkovic, and W. P. King, "Ultra-power-dense heat exchanger development through genetic algorithm design and additive manufacturing," *Joule*, vol. 5, no. 11, pp. 3045–3056, Nov. 2021, doi: 10.1016/j.joule.2021.08.004.

[44] N. N. Tušar, V. Kaučič, and N. Z. Logar, "Functionalized Porous Silicates as Catalysts for Water and Air Purification," in *New and Future Developments in Catalysis: Hybrid Materials, Composites, and Organocatalysts*, Elsevier B.V., 2013, pp. 365–383. doi: 10.1016/B978-0-444-53876-5.00017-9.

[45] "Chemistry and Physics of Fire and Liquid Fuels 4.1 DEFINITION OF FIRE 4.1.1 Basic Conditions A/ Fire Triangle," 2007.